The characterization of ancient Methanococcales malate dehydrogenases reveals that strong thermal stability prevents unfolding under intense γ-irradiation

D Madern, Frédéric Halgand, Chantal Houée-Levin, A-B Dufour, S Coquille, S Ansanay-Alex, S Sacquin-Mora, Celine Brochier-Armanet

The characterization of ancient *Methanococcales* malate dehydrogenases reveals that strong thermal stability prevents unfolding under intense γ-irradiation

Madern D.[1,*], Halgand F.[2], Houée-Levin C. [2], Dufour A-B.[3], Coquille S.[1], Ansanay-Alex S.[1], Sacquin-Mora S.[4], Brochier-Armanet C.[3,5,*]

1-Univ. Grenoble Alpes, CEA, CNRS, IBS, 38000 Grenoble, France

2-Université Paris Sud- CNRS, UMR 8000, bâtiments 201 P2 and 350, 91405, Orsay, France

3-Université Claude Bernard Lyon 1, CNRS, VetAgro Sup, Laboratoire de Biométrie et Biologie Évolutive, UMR5558, Villeurbanne, France

4-CNRS, Université de Paris, UPR 9080, Laboratoire de Biochimie Théorique, Paris, France ; Institut de Biologie Physico-Chimique-Fondation Edmond de Rothschild, PSL Research University, Paris, France.

5- Institut Universitaire de France (IUF)

* Corresponding authors : dominique.madern@ibs.fr, celine.brochier-armanet@univ-lyon1.fr

Abbreviations:

Ancestral sequence reconstruction (ASR)
Bootstrap values (BV)
Correspondence analysis (CA)
Lactate dehydrogenase (LDH)
Malate dehydrogenase (MalDH)
Melting temperature ($T_{M1/2}$)
OGT of the 18 strains of Methanococcales estimated from their proteome sequences according to the study by Lecocq et al. (2021) ($estOGT_{CORE-PROT}$)
OGT of the 18 strains of Methanococcales estimated from the sequences of the MalDH according to this study ($estOGT_{MalDH}$)
Optimal growth temperatures (OGT)
Optimal temperature for activity ($A\text{-}T_{opt}$)
Oxaloacetate (OAA)
Wild type (Wt)

Abstract

Malate dehydrogenases (MalDH) (EC.1.1.1.37), which are involved in the conversion of oxaloacetate to pyruvate in the tricarboxylic acid cycle, are a relevant model for the study of enzyme evolution and adaptation. Likewise, a recent study showed that *Methanococcales*, a major lineage of *Archaea*, is a good model to study the molecular processes of proteome thermoadaptation in prokaryotes. Here, we use ancestral sequence reconstruction and paleoenzymology to characterize both ancient and extant MalDHs. We observe a good correlation between inferred optimal growth temperatures (OGTs) and experimental optimal temperatures for activity (A-T_{opt}). In particular, we show that the MalDH present in the ancestor of *Methanococcales* was hyperthermostable and had an A-T_{opt} of 80°C, consistent with a hyperthermophilic lifestyle. This ancestor gave rise to two lineages with different thermal constraints, one remaining hyperthermophilic while the other underwent several independent adaptations to colder environments. Surprisingly, the enzymes of the first lineage have retained a thermoresistant behavior (i.e., strong thermostability and high A-T_{opt}), whereas the ancestor of the second lineage shows a strong thermostability, but a reduced A-T_{opt}. Using mutants, we mimic the adaptation trajectory towards mesophily and show that it is possible to significantly reduce the A-T_{opt} without altering the thermostability of the enzyme by introducing a few mutations. Finally, we reveal an unexpected link between thermostability and the ability to resist γ-irradiation-induced unfolding.

Keywords

Ancestral sequence reconstruction, extremophiles, thermal adaptation, irradiation, reactive oxygen species, COaLA evolutionary model.

Introduction

On Earth, environmental factors such as salinity, pH, redox potential, hydrostatic pressure, temperature, radiation, or desiccation, impose strong physical and chemical constraints on organisms, especially microorganisms (Rothschild and Mancinelli 2001; Pikuta, et al. 2007; Merino, et al. 2019). Coping with these constraints, which affect the structure, the dynamics and catalytic properties of all cellular components, requires specific adaptations (Coker 2019; Ando, et al. 2021; Knop, et al. 2023). For instance, it has been shown that the relative abundance of amino acids in proteins and proteomes is strongly correlated with the optimal growth temperature (OGT) of prokaryotes (Zeldovich, et al. 2007; Boussau, et al. 2008; Groussin and Gouy 2011; Lecocq, et al. 2021). However, other factors such as the environmental salinity or the guanine and cytosine content of genomes (genomic GC content) can also modulate the amino acid composition of proteomes (Dutta and Paul 2012; Vallina Estrada and Oliveberg 2022; Lamolle, et al. 2023; Amangeldina, et al. 2024). Disentangling the relative contribution of each factor is therefore challenging, as they may have antagonistic effects. As a result, the understanding of the precise substitution processes involved in proteome thermoadaptation remains elusive.

Paleoenzymology is a powerful tool for unravelling how amino acid substitutions have shaped enzyme properties during evolution. Indeed, by coupling bioinformatic ancestral sequence reconstruction (ASR) with laboratory enzyme resurrection, it is possible to experimentally characterize ancient enzymes from extinct organisms (Zaucha and Heddle 2017; Selberg, et al. 2021; Schwartz, et al. 2022). This approach has been used to address fundamental questions about evolution and to make inferences about paleoenvironments (Gaucher, et al. 2008; Perez-Jimenez, et al. 2011; Risso, et al. 2013; Akanuma 2017; Garcia, et al. 2017; Nguyen, et al. 2017; Blanquart, et al. 2021). However, ASR suffers from several biases (Williams, et al. 2006; Garcia and Kacar 2019). Among the many pitfalls, the most common is the use of inaccurate mathematical models of evolution. In particular, most current models are homogeneous, i.e., they assume that the substitution process is distributed homogeneously along the phylogeny and across the sites of the sequences, an assumption that is often violated by the data (Groussin, et al. 2013; Echave, et al. 2016; Naser-Khdour, et al. 2019; Del Amparo and Arenas 2022). Furthermore, most ASR models treat gaps as missing/ambiguous data or ignore them, despite their key role in protein evolution, and there is a real challenge to develop ASR models that efficiently account for indels (see for example (Jowkar, et al. 2023; Iglhaut, et al. 2024; Tule, et al. 2024) and references

therein). Furthermore, tracing the evolution of enzymes from very ancient ancestors is particularly difficult because the phylogenetic signal contained in the sequences is progressively eroded over time (Gribaldo and Philippe 2002). Thus, the uncertainty in ancestral reconstructions increases with the age of the ancestors under study. Finally, the number of genes / proteins that can be studied over large evolutionary scales is very limited because the size of core gene repertoires decreases with increasing phylogenetic distance (Touchon, et al. 2020).

For prokaryotes, the relationship between OGT and amino acid abundance in proteomes has been used to build molecular thermometers (Zeldovich, et al. 2007; Boussau, et al. 2008; Groussin and Gouy 2011; Smole, et al. 2011; Sauer and Wang 2019; Lecocq, et al. 2021; Kurokawa, et al. 2023). These have been used to infer ancestral OGTs of key ancestors in the Tree of Life (Boussau, et al. 2008; Groussin and Gouy 2011; Eme, et al. 2023), and some of these predictions have been experimentally tested in the laboratory (Gaucher, et al. 2003; Gaucher, et al. 2008; Lu, et al. 2024). Surprisingly, in many cases the resurrected ancestral proteins exhibit unexpectedly strong stability, in particular high thermostability (Akanuma 2017; Garcia and Kacar 2019). However, whether these observations reflect the true evolutionary trends or are the result of ASR artefacts is still open to debate (Trudeau, et al. 2016; Wheeler, et al. 2016).

Methanogens have a wide range of OGTs, making their study very useful for understanding the thermal adaptation process of enzymes (Prondzinsky, et al. 2023). Among these, the *Methanococcales* are particularly interesting, as it has recently been shown that the OGT alone explains 70% of the variance in amino acid abundance in proteomes, whereas in almost all studies the genomic GC content is the dominant factor (Lecocq, et al. 2021). This is explained by the fact that the genomic GC content is very stable in this archaeal order, whereas the OGTs vary widely (from 35°C for *Methanococcus* vannielii SB to 90°C for *Methanocaldococcus* sp. FS406 22). Using ASR methods, Lecocq et al. (2021) showed that several methanococcales species have independently adapted to moderate environments from (hyper)thermophilic ancestors. They also found that amino acid substitution is the main driver of thermoadaptation, sequentially shaping the amino acid composition of proteomes, with lysine playing a key role in the process (Lecocq, et al. 2021).

In this follow-up study, we used ASR to investigate how evolution has refined the temperature-dependent properties of methanococcales enzymes in response to changes in the OGT. We used the NAD(P)H-dependent malate dehydrogenases (MalDHs) (EC 1.1.1.37) because they are relevant

models to study the mechanisms of evolution and extremophilic adaptation of enzymes (Richard, et al. 2000; Dalhus, et al. 2002; Madern 2002; Irimia, Madern, et al. 2004; Irimia, Vellieux, et al. 2004; Tehei, et al. 2005; Coquelle, et al. 2007; Kawakami, et al. 2009; Coquelle, et al. 2010; Kalimeri, et al. 2014; Roche, et al. 2019; Katava, et al. 2020; Blanquart, et al. 2021; Brochier-Armanet and Madern 2021; Iorio, et al. 2021). MalDHs belong to the large super-family of Lactate/Malate Dehydrogenases (LDH/MalDH) (Birktoft, et al. 1982; Boucher, et al. 2014; Brochier-Armanet and Madern 2021; Robin, et al. 2023). They are involved in the tricarboxylic acid cycle by converting oxidized oxaloacetate (OAA) to malate, using either NADH or NADPH as a coenzyme, whereas LDH are involved in the anaerobic metabolism of glucose by catalysing the conversion of pyruvate to lactate. Regarding the oligomeric state, MalDHs are found as homodimers or homotetramers (Talon, et al. 2014; Roche, et al. 2019; McCue and Finzel 2022). We found that the ancestral OGTs of *Methanococcales* inferred from MalDH sequences are consistent with those obtained from core protein families (Lecocq, et al. 2021). As a first step, we inferred the phylogeny of present-day *Methanococcales* MalDH and used it to predict the ancestral MalDH sequences. We then analyzed the effect of temperature on the conformational stability and catalytic activity of MalDH at key positions of the phylogeny. We showed that the ancestral MalDHs display strong conformational stability, as do the present-day MalDHs from hyperthermophiles, but their enzymatic activity profiles differ. Analysis of the substitution trajectories across the MalDH sequences provided interesting clues as to how the mesophilic properties might have evolved from hyperthermophilic ancestors. This was tested experimentally by using the *Methanocaldococcus jannaschii* MalDH (*M. jann* MalDH) as a scaffold. Finally, as a recent work on LDH has shown a link between the thermal stability of LDHs and their ability to resist unfolding induced by γ-rays irradiation (Halgand, et al. 2020), we tested the response of some ancestral and modern MalDHs when exposed to γ irradiation. We found that these enzymes remained folded even when they accumulated numerous oxidative damages due to high doses of irradiation. Taken together, our data support a strong link between resistance to thermal and oxidative stress. They also show that such a peculiar phenotype is an ancient trait.

Results

1) Evolution of MalDH from Methanococcales

We assembled a dataset encompassing the MalDH sequences from the 18 strains of *Methanococcales* from the study by Lecocq et al. (2021) and seven strains of *Methanomada* used as outgroup. Although it is based on the analysis of a single protein and therefore on a limited number of amino acid positions, the MalDH phylogeny is overall well supported (most Bootstrap Values (BV) > 90%) and consistent with the current taxonomy (Fig. 1). In particular, the monophyly of the families *Methanocaldococcaceae* and *Methanococcaceae*, and genera *Methanocaldococcus* and *Methanotorris* is recovered, while, as in most studies, *Methanothermococcus* and *Methanococcus* strains are mixed in the tree (see for instance (Takai, et al. 2002; Kendall, et al. 2006; Sakai, et al. 2019; Lecocq, et al. 2021)). This recurring observation urges the need to redefine the contours of these two genera. The first speciation event in the MalDH phylogeny separates *Methanocaldococcaceae* (i.e., *Methanocaldococcus* and *Methanotorris*, BV = 59%) from *Methanococcaceae* (*Methanothermococcus* and *Methanococcus*, BV = 91%). With respect to OGTs, the described *Methanocaldococcus* are all hyperthermophilic (OGT ≥ 80°C), *Methanotorris* are either thermophilic (i.e., *Methanotorris formicicus*, OGT = 75°C) or hyperthermophilic (i.e., *Methanotorris igneus*, OGT = 88°C), the two *Methanothermococcus* are thermophilic (45°C < OGT < 80°C) and *Methanococcus* are either slightly thermophilic (i.e., *Methanococcus aeolicus*, OGT = 46°C) or mesophilic (all other *Methanococcus*, OGT ≤ 45°C) (Fig.1).

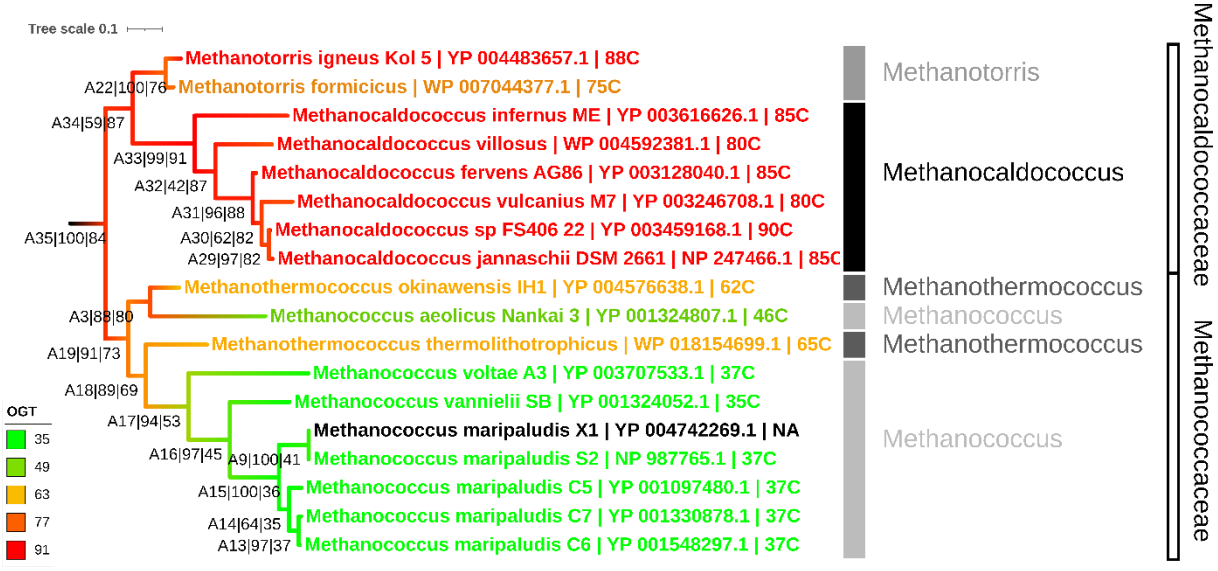

Fig. 1. Rooted maximum likelihood phylogeny of MalDH from *Methanococcales*. For clarity the outgroup is not shown. The full rooted tree (including the seven strained used as outgroup) is provided as Supplementary Fig. S1. Taxonomic information is indicated with vertical bars: grey bars correspond

to the genera (i.e., *Methanococcus*, *Methanocaldococcus*, *Methanotorris*, *Methanothermococcus*), white bars to the families (i.e., *Methanocaldococcaceae* and *Methanococcaceae*). Numbers at nodes correspond to ancestor names | bootstrap_values | estimated_OGT_with_the_standard_linear_model (see below). The scale bar corresponds to the average number of substitutions per site. Colours of strains correspond to OGT from the literature (Huber, et al. 1982; Jones, et al. 1983; Burggraf, et al. 1990; Jeanthon, et al. 1998; Takai, et al. 2002; Takai, et al. 2004; Kendall, et al. 2006; Mehta and Baross 2006; Bellack, et al. 2011; Whitman, et al. 2015) (see also Supplementary Table S1). Branch colours correspond to inferred ancestral OGTs along the phylogeny.

To test whether there is a correlation between the amino acid content of MalDH sequences and the OGT of strains, we performed a correspondence analysis (CA). We found that the first two axes explained 70.5% of the observed variance (first axis: 53.4% and second axis: 17.1%, Fig. 2A), whereas the third axis explained only 8.2% of the variance (not shown). We also observed that OGT strongly correlated with the MalDH sequence scores on the first axis of the CA (Fig. 2B, $r = -0.928$, pvalue = 1.3×10^{-07}), but not with the second axis ($r = 0.158$, pvalue = 0.5451) nor the third axis ($r = -0.048$, pvalue = 0.8534). These results are consistent with those obtained on the complete proteomes and core proteins of *Methanococcales* (Lecocq, et al. 2021), which means that in these archaea, the signal associated with thermoadaptation is strong enough to be observed at the level of a single protein. We also observed a significant but slightly weaker correlation between OGT and the amount of I, V, Y, R, E, L amino acids in MalDH sequences ($r = 0.826$, pvalue = 4.4×10^{-05}, Fig. 2C), which has been proposed as a good predictor of OGT (Zeldovich, et al. 2007). Regarding MalDH gene GC content, we did not find any significant correlation with any of the first three axes of the CA (all pvalues > 0.05, not shown) nor with the OGT ($r = -0.312$, pvalue = 0.2234, not shown).

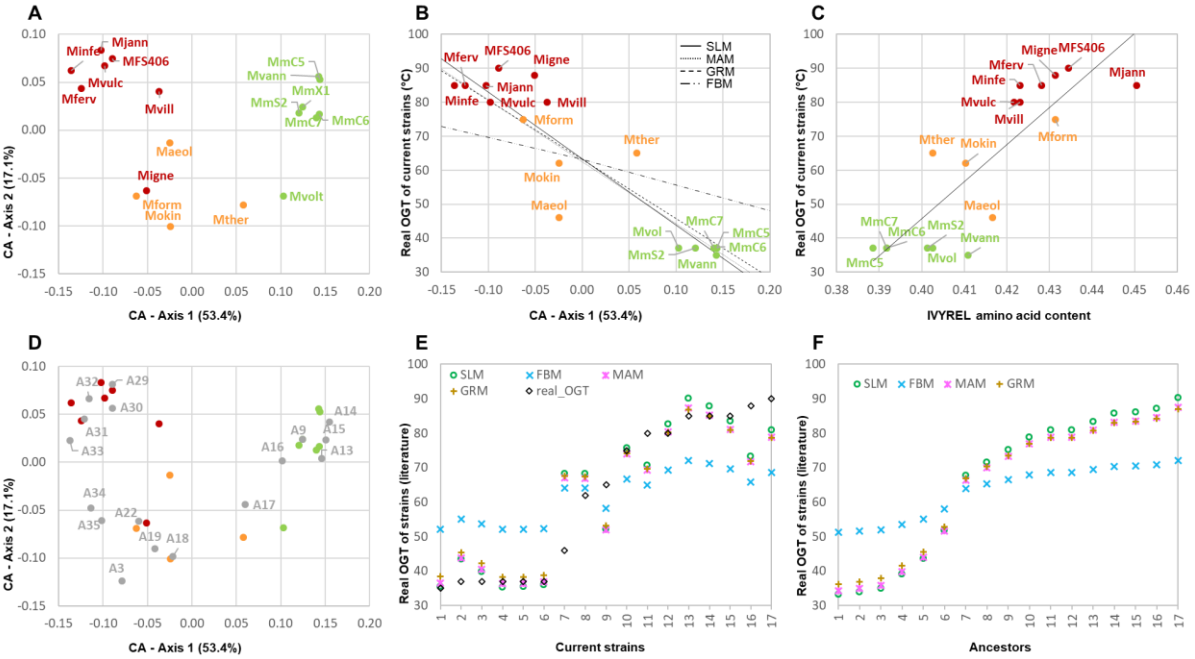

188

189

190 **Fig. 2. Analysis of the signal contained in MalDH sequences.** The dots on panels A-D represent
191 MalDH sequences from the studied *Methanococcales* strains and their ancestors, while the marks on
192 panels E and F represent estOGT$_{MalDH}$ with different linear models. Present-day hyperthermophiles are
193 shown in red (Migne = *Methanotorris igneus* Kol_5, Mvulc = *Methanocaldococcus vulcanius* M7,
194 Mvill = *Methanocaldococcus villosus*, MFS406 = *Methanocaldococcus* sp. FS406-22,
195 Mjann = *Methanocaldococcus jannaschii* DSM2661, Minfe = *Methanocaldococcus infernus* ME,
196 Mferv = *Methanocaldococcus fervens* AG86), thermophiles in orange (Mform = *Methanotorris*
197 *formicicus*, Mther = *Methanothermococcus thermolithotrophicus*, Mokin = *Methanothermococcus*
198 *okinawensis* IH1, Maeol = *Methanococcus aeolicus* Nankai-3), and mesophiles in green
199 (Mvann = *Methanococcus vannielii* SB, MmS2 = *Methanococcus maripaludis* S2,
200 MmC7 = *Methanococcus* maripaludis C7, MmC6 = *Methanococcus maripaludis* C6,
201 MmC5 = *Methanococcus maripaludis* C5, Mvolt = *Methanococcus voltae* A3), while ancestors are in
202 gray. **(A)** Representation of the first two axes of the correspondence analysis (CA), which explained
203 70.5% of the observed variance in amino acid content. The first axis explains 53.4% of the variance and
204 the second 17.1%. **(B)** Correlation between OGT of the strains and scores of their MalDH sequences
205 on the first axis of the correspondence analysis CA ($r = -0.928$, pvalue = 1.3×10^{-07}) according to the
206 standard linear model (SLM). Other lines correspond to the models by Martins and Hansen (MAM), by
207 Grafen (GRM), and by Felsenstein (FBM). **(C)** Correlation between the OGT of the strains and the I, V,

Y, R, E, L amino acid content of their MalDH sequences according to a SLM (r = 0.826, pvalue = 4.4×10^{-05}). **(D)** Representation of the first two axes of the (CA) including both present-day methanococcales strains and their ancestors. **(E)** Estimated OGT ($estOGT_{MalDH}$) of present-day strains according to the scores of their MalDH on axis 1 of the CA using standard linear model (SLM), and models by Martins and Hansen (MAM), by Grafen (GRM), and by Felsenstein (FBM). Real OGTs according to the literature are indicated by empty black diamonds. Numbers on the X-axis correspond to strains: 1=Mvann, 2=Mvolt, 3=MmS2, 4=MmC5, 5=MmC6, 6=MmC7, 7=Maeol, 8=Mokin, 9=Mther, 10=Mform, 11=Mvill, 12=Mvulc, 13=Minfe, 14=Mferv, 15=Mjann, 16=Migne, and 17=MFS406. **(F)** $EstOGT_{MalDH}$ of ancestors according to the scores of their MalDH on axis 1 of the CA using the standard linear model (SLM), and models by Martins and Hansen (MAM), by Grafen (GRM), and by Felsenstein (FBM). Numbers on the X-axis correspond to ancestors: 1=A14, 2=A15, 3=A13, 4=A9, 5=A16, 6=A17, 7=A18, 8=*Methanococcaceae*/A19, 9=A22, 10=A3, 11=A29, 12=A30, 13=LMCA/A35, 14=*Methanocaldococcaceae*/A34, 15=A32, 16=A31, and 17=A33. Confidence intervals and numeric values of $EstOGT_{MalDH}$ are provided as Supplementary Fig. S2 and Table S2, respectively.

We then used the correlation between the OGT of present-day methanococcales strains and the scores of MalDH sequences on the first axis of the CA to construct molecular thermometers. We used four models, the standard linear model and three regression models that account for the phylogenetic relationships between MalDH sequences (i.e., the Grafen model, the Martins and Hansen model, and the Felsenstein Brownian model, see Methods). The first two provided a regression similar to the standard model, while the slope of the Felsenstein Brownian model was weaker (Fig. 2B). To test the reliability of the thermometer, we used the regression lines to predict the OGT of current methanococcales strains (referred to as $estOGT_{MalDH}$). Estimations performed with the linear, the models by Grafen and by Martins and Hansen were close to the real OGTs, excepted for four strains (i.e., Maeol, Migne, Mther, and MFS406, Fig. 2E) Interestingly, the OGTs of three of these strains were difficult to predict, even when all core proteins were considered (Lecocq, et al. 2021). In contrast, the Felsenstein model tended to underestimate high OGTs and overestimate low OGTs (Fig. 2E and Supplementary Fig. S2 and Table S2). Taken together, these results suggest that although the standard model does not account for phylogenetic relationships between sequences, it is not biased by them. Determining the reasons why the Brownian model produced different results is beyond the scope of this study.

Then, we applied these models to the ancestral MalDH sequences to predict the OGT of the corresponding ancestors. Again, the standard linear model, the model by Grafen, and the model by Martins and Hansen provided very close OGT estimates (Figs. 2D, 2F, and Supplementary Fig. S2 and Table S2). Since the standard linear model and two of the three models accounting for phylogenetic relationships between strains gave very similar results, for the rest of the analysis $estOGT_{MalDH}$ will refer to the OGTs estimated from the MalDH sequences using the standard linear model. In line with these inferences, the ancestor of the *Methanococcales* was predicted to be slightly hyperthermophilic (LMCA/A35, $estOGT_{MalDH}$ = 84°C, Fig. 1), as was the ancestor of the *Methanocaldococcaceae* (A34, $estOGT_{MalDH}$ = 87°C, Fig. 1). Subsequently, a decrease in OGT was observed at the base of the genus *Methanotorris* (A22, $estOGT_{MalDH}$ = 76°C), followed by a significant increase in *Methanotorris igneus* (OGT = 88°C), and a more moderate increase in *Methanotorris formicicus* (OGT = 75°C) (Fig. 1). In the ancestor of the genus *Methanocaldococcus*, an increase in OGTs was observed (A33, $estOGT_{MalDH}$ = 91°C), whereas in the *Methanococcaceae*, very different trends were observed (Fig. 1). From a thermophilic ancestor (A19, $estOGT_{MalDH}$ = 73°C), two independent adaptations toward cooler temperatures occurred in the lineage leading to *Methanococcus aeolicus* (OGT = 46°C) and in the lineage leading to *Methanococcus voltae*, *Methanococcus vannielii*, and *Methanococcus maripaludis* (OGTs = 35-37°C), while OGTs remained almost unchanged in the two *Methanothermococcus* lineages (OGTs = 62 and 65°C, Fig. 1).

2) Success and failure in methanococcales MalDHs purification

Over the years, we have developed overexpression and purification procedures that are routinely used to obtain pure recombinant MalDH from various organisms, including mesophiles (Richard, et al. 2000; Dalhus, et al. 2002; Madern 2002; Irimia, Madern, et al. 2004; Irimia, Vellieux, et al. 2004; Tehei, et al. 2005; Coquelle, et al. 2010; Kalimeri, et al. 2014; Roche, et al. 2019; Katava, et al. 2020; Blanquart, et al. 2021; Brochier-Armanet and Madern 2021; Iorio, et al. 2021). Here, we successfully purified the MalDH from *Methanococcus infernus, Methanocaldococcus jannaschii, Methanotorris formicicus, Methanopyrus kandleri* (outgroup), and *Methanothermobacter thermautotrophicus* (outgroup). However, we encountered major difficulties in purifying MalDH from both present-day and ancestral mesophilic methanococcales (see below), which prevented their experimental characterization. We tried several overexpression protocols, overexpression plasmids, and different *E. coli* strains. Unfortunately, none of the tests yielded sufficient amounts of soluble enzyme. We also tried refolding procedures, but to no

avail. This is particularly intriguing as we have had no difficulty in producing MalDH from mesophiles belonging to other taxonomic groups. This suggests that in mesophilic methanococcales, MalDH may follow a specific chaperone-assisted folding pathway, which cannot be mimicked within the *E. coli* cytoplasm. Fortunately, when expressed in *E. coli*, the MalDH sequences inferred in the three deepest methanococcales ancestors (LMCA/A35, *Methanocaldococcaceae*/A34, and *Methanococcaceae*/A19) and two intermediate ancestors A30 and A33 were correctly folded and soluble, allowing the appropriate purification procedure to be set up as indicated in the Materials and Methods section. At the end of the purification, the tetrameric state was assessed using either a calibrated size exclusion chromatography column or analytical centrifugation (Supplementary Fig. S3-S5). With the LMCA/A35 MalDH, we found that in addition to the tetramer, a fraction of the enzyme exists as an octamer.

3) Thermal-dependent conformational stability of the ancestral methanococcales MalDHs.

In the first part of this work, we addressed the question concerning the thermal properties of enzymes at the root of *Methanococcales.* To achieve this goal, we monitored the circular dichroism (CD) spectra of the three deepest ancestral MalDHs, i.e., the ancestors of all *Methanococcales* (LMCA/A35), *Methanocaldococcaceae* (A34), and *Methanococcaceae* (A19), before and after incubation at 90°C to test their conformational thermostability. In parallel, we used the LDH of the bacterium *Selenomonas ruminantium* (Bertrand, et al. 2023) and the MalDH of *M. kand* as control proteins representative of mesophiles and hyperthermophiles, respectively (Fig. 3A-B). The CD spectra of the three ancestral enzymes, *M. kand* MalDH and *S. rumi* LDH recorded at 25°C are typical of folded proteins, with a strong negative molar ellipticity below 200 nm and a peak with positive values centered at 195 nm (Fig. 3B-E, black diamonds). After incubation at 90°C, MalDH CD spectra remained unchanged, demonstrating that the three ancestral MalDHs exhibit behavior typical of modern hyperthermophilic MalDHs (Fig. 3B-E, red diamonds). Remarkably, the spectrum of the *S. rumi* LDH observed after incubation at 60°C is already modified, indicating that the thermal treatment has strongly altered the folding state of the enzyme (Fig. 3A, black and red diamonds).

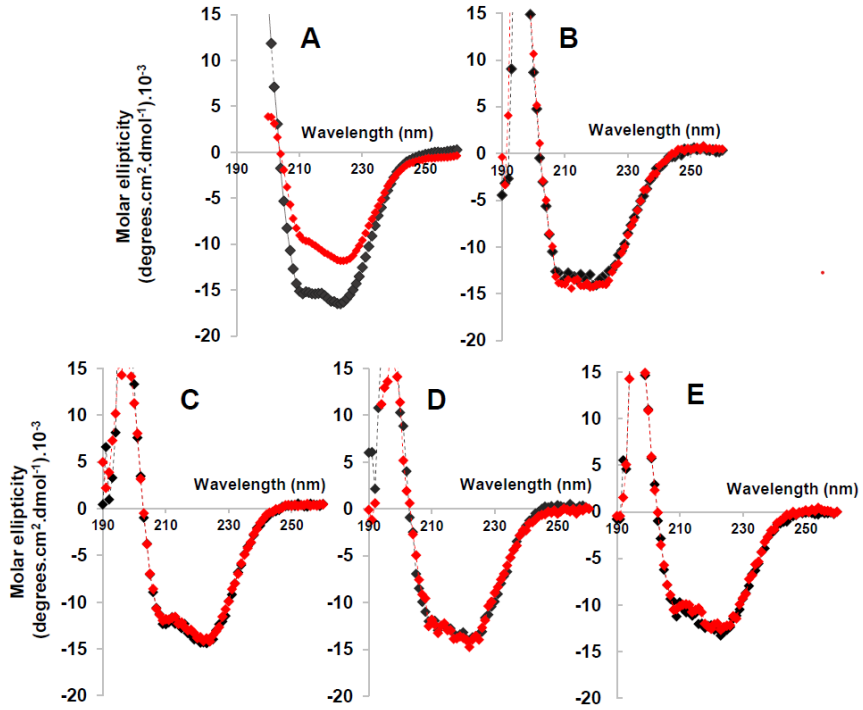

Fig. 3. Effect of temperature on the circular dichroism (CD) spectra on the three deepest *Methanococcales* ancestral MalDHs and controls. Curves correspond to CD spectra taken at 25°C before the thermal treatment (TT) (black diamonds) and after the thermal treatment (red diamonds). **(A)** *S. rumi* LDH, TT = 60°C (OGT = 37°C). **(B)** *M. kand* MalDH, TT = 90°C (OGT = 98°C). **(C)** Ancestor of *Methanococcales* MalDH (LMCA/A35, $estOGT_{MalDH}$ = 84°C), TT = 90°C. **(D)** Ancestor of *Methanocaldococcaceae* MalDH (A34, $estOGT_{MalDH}$ = 87°C), TT = 90°C. **(E)** Ancestor of *Methanococcaceae* MalDH (A19, $estOGT_{MalDH}$ = 73°C), TT = 90°C.

To test whether the hyperthermophilic modern and ancestral enzymes could be unfolded, we added 10% v/v of pure HCl to the 300 µL of sample in the cuvette used for CD and incubated for an additional 15 min at 70°C. The resulting spectra showed a strong loss of the negative molar ellipticity, indicating that the three ancestral MalDHs tested unfold after application of such a stringent treatment (Supplementary Fig. S6). The CD spectrum of *M. kand* MalDH was less affected, suggesting that the enzyme is more resistant to the treatment (Supplementary Fig. S6A). Altogether, this suggests that the three deepest *Methanococcales* ancestral MalDHs are hyper thermostable and require drastic treatment to unfold.

We also recorded the stability of these enzymes using residual activity measurements (see Methods). This method is commonly used to evaluate the effect of a chemical-physical treatment on the functionality of MalDH and LDH enzymes (Coquelle, et al. 2007; Coquelle, et al. 2010; Blanquart, et al. 2021; Robin, et al. 2023). The method allows to extract the apparent melting temperature ($T_{M1/2}$), i.e., the temperature at which 50% of the enzyme is still active.

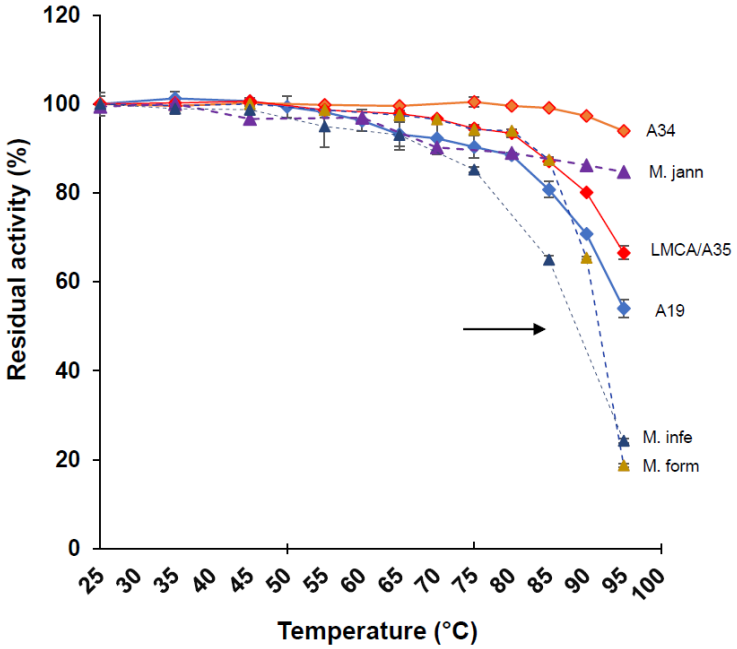

Fig. 4. MalDH thermostability probed by residual activity measurement. Present day and ancestral MalDHs are indicated by triangles and diamonds, respectively. MalDH of *M. jann* (OGT = 85°C) is in dark purple, *M. form* (OGT = 75°C) in brown, *M. infe* (OGT = 85°C) in dark blue, while the MalDH of the ancestor of *Methanococcales* (LMCA/A35, $estOGT_{MalDH}$ = 84°C) is in red, *Methanocaldococcaceae* (A34, $estOGT_{MalDH}$ = 87°C) in orange, and *Methanococcaceae* (A19, $estOGT_{MalDH}$ = 73°C) in cyan. The arrow designates $T_{M1/2}$.

Here, we tested the ancestral MalDHs at the root of the *Methanococcales* (LMCA/A35, $estOGT_{MalDH}$ = 84°C), *Methanocaldococcaceae* (A34, $estOGT_{MalDH}$ =°87°C), and *Methanococcaceae* (A19, $estOGT_{MalDH}$ = 73°C), as well as those from three present-day species: *M. form* (OGT = 75°C), *M. jann* (OGT = 85°C), and *M. infe* (OGT = 85°C). We found that these six MalDHs had $T_{M1/2}$ values above 90°C (Fig. 4), demonstrating that they behave as hyper thermostable enzymes. Note that the *M. infe* MalDH profile suggested a slightly lower resistance to high temperature, probably due to differences in

329 the kinetic processes leading to deactivation and unfolding. However, the full characterization of these
330 processes is beyond the scope of this study.
331 We concluded that at the root of the *Methanococcales,* the LMCA/A35 MalDH had a strong
332 conformational stability that allowed it to resist to unfolding induced by the high environmental
333 temperature. This correlates well with estimated ancestral OGTs, which suggests that ancestor
334 LMCA/A35 was hyperthermophilic ($estOGT_{MalDH}$ = 84°C, Fig.1). This ancestral phenotype was
335 conserved in the ancestor of *Methanocaldococcaceae* (A34), whose present-day descendants live in
336 hot ecological niches (Fig. 1). This suggests that the amino acid substitutions that occurred in MalDH
337 sequences in this lineage were quite neutral with respect to thermostability. More surprisingly, this
338 characteristic was also conserved in *M. form*, which has been characterized as thermophilic (Takai, et
339 al. 2004), and in the ancestor of the *Methanococcaceae*, which we predicted to be thermophilic (A19,
340 $estOGT_{MalDH}$ = 73°C).
341 With regard to adaptation to lower environmental temperatures, the inability to purify mesophilic MalDH
342 prevents us from drawing definitive conclusions about the changes in conformational stability that may
343 have accompanied these changes in OGT. However, two scenarios can be suggested. First, one could
344 hypothesize that both the conformational stability and the activity of MalDHs were reduced during the
345 OGT shifts. Alternatively, it is possible that the high conformational thermal stability was maintained
346 while the activity profile was shifted to lower temperatures. According to the first hypothesis, the
347 substitutions that occurred at the basis of the mesophilic lineages must have had an effect on both the
348 conformational stability and the activity of MalDH. In the second case, these substitutions must only
349 have affected the activity and not the conformational stability of MalDH.
350
351 **4) Temperature dependence of enzymatic activity**.
352 Amino acid substitutions can affect not only conformational stability, but also the dynamic properties of
353 an enzyme and, by extension, its catalytic properties (Yu and Dalby 2018; Bigman and Levy 2020).
354 Therefore, we recorded the enzymatic activity of several present-day and ancestral MalDHs at different
355 temperatures: the MalDH of the three deepest ancestors (LMCA/A35, *Methanocaldococcaceae*/A34 and
356 *Methanococcaceae*/A19), two intermediate ancestors along the hyperthermophilic *Methanocaldococcus*
357 lineage (A33 and A30), and three present-day *Methanocaldococcaceae* species (*M. jann*, *M. infe*, and

M. form) (Fig. 5). The profiles of two MalDHs from *M. kand* and *M. therm*, both belonging to the outgroup, were also recorded.

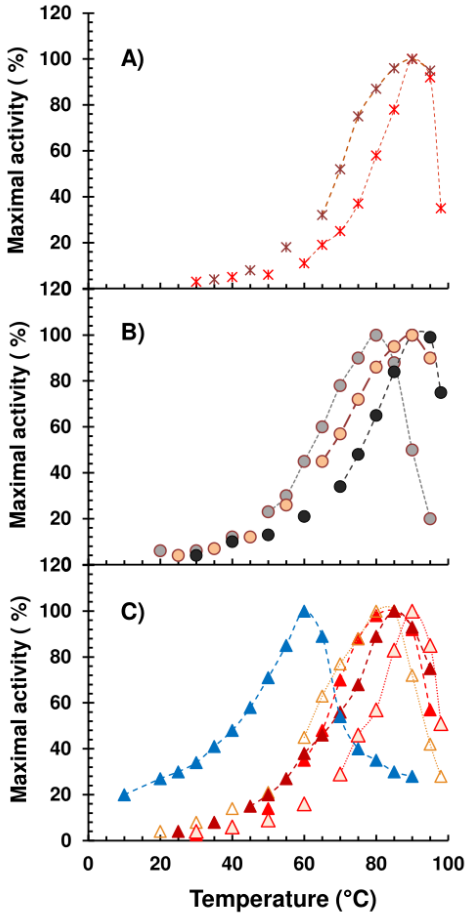

Fig 5. Plot of the relative activity as a function of temperature. The averaged values are expressed as % of activity relative to the maximal value recorded for each enzyme. For a given MalDH, optimal temperature for activity (A-T_{opt}) corresponds to the peak of the curve, i.e., the maximal value recorded. **(A)** Enzymes from the outgroup: MalDH from *M. kand* (OGT = 98°C, red crosses, A-T_{opt} = 90°C) and *M. ther* (OGT = 65°C, brown crosses, A-T_{opt} = 90°C). **(B)** Present-days enzymes: MalDH from *M. jann* (OGT = 85°C, black circles, A-T_{opt} = 93°C), *M. form* (OGT = 75°C, orange circles, A-T_{opt} = 90°C), *M. infe* (OGT = 85°C, grey circles, A-T_{opt} = 80°C). **(C)** Ancestral enzymes: MalDH from the *Methanococcales* ancestor (LMCA/A35, estOGT$_{MalDH}$ = 84°C, closed red triangles, A-T_{opt} = 80°C), the *Methanocaldococcaceae* ancestor (A34, estOGT$_{MalDH}$ =87°C, dark brown triangles, A-T_{opt} = 81°C), two intermediate ancestors within the *Methanocaldococcus* lineage (A33, estOGT$_{MalDH}$ = 91°C, open red triangles, A-T_{opt} = 91°C and A30, estOGT$_{MalDH}$ = 82°C, open orange triangles, A-T_{opt} = 82°C,

372 respectively), and the *Methanococcaceae* ancestor (A19, estOGT$_{MalDH}$ = 73°C, blue triangles, A-
373 T$_{opt}$ = 67°C).
374
375 The profiles showed that all enzymes from modern (hyper)thermophilic organisms, i.e., *M. jann*, *M. infe*,
376 *M. form*, *M. ther*, and *M. kand* had the expected typical profile with an optimal temperature for activity
377 (A-T$_{opt}$) in the range 80-95°C, and a relative activity decreasing to 20% in the range 50-65°C (Fig.5).
378 The enzymatic activity for the LMCA/A35 and *Methanocaldococcaceae*/A34 MalDHs showed equivalent
379 profiles, demonstrating that they were fully functional at high temperature. In contrast, the enzymatic
380 profile of the MalDH inferred in the *Methanococcaceae* ancestor (A19) was strongly shifted towards
381 lower temperatures, with an A-T$_{opt}$ of 60°C. In this case, the threshold temperature for maintaining 20%
382 of the activity was 15°C. This suggested that in the ancestor of the *Methanococcales* (LMCA/A35,
383 estOGT$_{MalDH}$ = 84°C), MalDH exhibited both strong conformational stability and enzymatic activity at
384 high temperature, two characteristics that were conserved in the *Methanocaldococcaceae* lineage (A34,
385 A33, A30, *M. jann*, *M. infe,* and *M. form*, all estOGT$_{MalDH}$/OGT ≥ 75°C), independently of amino acid
386 substitutions that may have occurred in the MalDH sequences. In contrast, the MalDH inferred in the
387 ancestor of *Methanococcaceae* (A19, estOGT$_{MalDH}$ = 73°C) showed a decoupling between its
388 conformational stability and its enzymatic activity. This suggested that the 13 amino acid substitutions
389 that occurred in the stem of *Methanococcaceae*, i.e., along the branch linking ancestors A35 and A19,
390 resulted in an enzyme that was still hyperthermostable, but with optimal activity at more moderate
391 temperatures.
392 For many years the activity/stability trade-off was the dominant concept to explain thermal adaptation of
393 enzymes (Goldstein 2011). It implies that mesophilic and psychrophilic enzymes must sacrifice their
394 stability to achieve an increase in conformational flexibility crucial for activity. This point of view has been
395 challenged by two studies based on ASRs of the adenylate kinase and the 3-isopropylmalate
396 dehydrogenase (Nguyen, et al. 2017; Furukawa, et al. 2020). In particular, it was shown that their
397 ancestral states were both thermostable and catalytically efficient at low temperature. Our data based
398 on MalDH confirmed that a catalytic activity at moderate temperature can be observed on a thermally
399 stable scaffold. Crystallographic investigations using the ancestral MalDHs from *Methanococcales* are
400 currently under way and will help to analyze this phenomenon.
401

5) Does OGT and A-T_{opt} correlate?

One of the aims of the study was to investigate the extent to which the ancestral $estOGT_{MalDH}$ and the A-T_{opt} correlated. The measurements of A-T_{opt} for all the enzymes studied here, were done at a concentration of 0.8 mM OAA. Such a value was a compromise (i) to ensure a non-limiting effect of OAA concentration at the beginning of the reaction and (ii) to avoid inhibition by high OAA concentration. Determination of the optimal OAA value for each enzyme and at different temperatures in order to gain in A-T_{opt} accuracy was beyond the scope of this study. Furthermore, the experimental determination of A-T_{opt} is difficult, particularly at high temperatures, and requires the use of temperature-controlled apparatus, so we assumed that all values are within a confidence limit of +/- 5°C. The results are shown in Table 1. The OGT and MalDH A-T_{opt} values of *M. kand* (outgroup), *M. infe*, and *M. jann* were close to each other. For the thermophilic *M. ther* (outgroup) and *M. form*, OGT values were higher than the A-T_{opt} of their MalDHs. We cannot exclude that the experimental OGT was underestimated for these two species. This could indeed be the case for the M. form, where the OGT could actually be close to 80°C. (Philippe Oger and Priscilla Gillet, personal communication) For the resurrected ancestral MalDHs, we observed almost identical values for the inferred OGT and A-T_{opt}. This is particularly noticeable with the A-T_{opt} of the MalDH inferred at the root of the *Methanococcaceae* (A19) lineage (A-T_{opt} = 60°C), which is consistent with the strong shift towards low OGT predicted using molecular thermometers applied to MalDHs ($estOGT_{MalDH}$ = 73°C, this study) and proteomes ($estOGT_{MalDH}$ = 64.5/65°C) (Lecocq, et al. 2021).

Table 1. Table showing OGTs according to data from the literature, estimated OGTs from proteome sequences ($estOGT_{CORE-PROT}$) (Lecocq, et al. 2021), estimated OGT from MalDH protein sequences ($estOGT_{MalDH}$, this study), and experimentally determined A-T_{opt} (this study), for two outgroup species: *M. kand* (*Methanopyrales*) and *M. ther* (*Methanobacteriales*), three present-day species of *Methanococcales*: *M. jann*, *M. infe*, *M. form*, and five methanococcales ancestors: LMCA/A35, *Methanocaldococcaceae*/A34, *Methanococcaceae*/A33, and two intermediate ancestors along the *Methanocaldococcaceae*: A30, and A19.

Taxa	Experimental OGT (°C)	$estOGT_{CORE-PROT}$ (°C)	$estOGT_{MalDH}$ (°C)	Experimental A-T_{opt} (°C)
Outgroup				
M. kand	98 (Kurr, et al. 1991)	-	-	90
M. ther	65 (Zeikus and Wolfe 1972)	-	-	90
Methanococcales				
M. jann	85 (Jones, et al. 1983)	85-90	-	90
M. infe	85 (Jeanthon, et al. 1998)	90-93	-	80

M. form	75 (Takai, et al. 2004)	75-86	-	90
LMCA, A35	-	81-83	**84**	85
A34	-	NA	**87**	85
A33	-	84-86	**91**	90
A30	-	NA	**82**	80
A19	-	64.5-65	**73**	**60**

6) Mimicking mesophilic adaptation.

To overcome the inability to purify MalDH from present-day mesophilic Methanococcales, we applied a mimicry strategy based on a sequence comparison between MalDH sequences from the hyperthermophilic *M. jann*, for which a structure exists (Protein data bank, PDB accession number,1HYG), and the mesophilic *M. mari* C7. In fact, it is well known that present day hyperthermophilic proteins have an increased number of salt-bridges compared to their mesophilic and psychrophilic counterparts (see (Coquelle, et al. 2007; Pinney, et al. 2021) and references therein). For example, in proteins from hyperthermophiles, E and R amino acids are preferentially used over D and K, because they have longer side chains that can form ionic interactions with more partners and complex networks of salt bridges that greatly increase the thermal stability of the proteins (Donald, et al. 2011; Sammond, et al. 2016). This is also the case for MalDH, where the *M. mari* enzyme contains 21 E and 11 R, whereas the *M. jann* protein contains 27 E and 18 R (Supplementary Table S2). Other studies suggested that G and P amino acids play a role in the thermal adaptation of enzymes to low temperatures (Feller 2010; Michetti, et al. 2017). This is due to their opposite influence on conformational dynamics: G, which lacks a β carbon, has the highest degree of conformational entropy, whereas P can sample only a few states and has the lowest degree of conformational entropy (Prajapati, et al. 2007; Feng, et al. 2020). The ability to increase the thermostability of enzymes by adding P residues to their sequences has been successfully exploited (Goihberg, et al. 2007; Tian, et al. 2010; Zhou, et al. 2010). To test the impact of these residues, we designed two mutants using the hyperthermophilic Wild-type (Wt) *M. jann* MalDH as a template.

```
                                                13                  1   2          14
M.mari C7WT       MEVSIIGASGKIGSVLSLLLAKESYIKNINLIARNGSINKLKGLKMDLYDAMAAAGQDTN
M.jann WT         MKVTIIGASGRVGSATALLLAKEPFMKDLVLIGREHSINKLEGLREDIYDALAGTRSDAN
M.jann C7like     MKVTIIGASGRVGSATALLLAKEPFMKDLVLIGREHSINKLKGLRMDIYDALAGTRSDAN
M.jann C7likeGP   MKVTIIGASGRVGSATALLLAKESFMKDLVLIGREHSINKLKGLRMDIYDALAGTGSDAN
                            10        *         *         *         *         *

                                              15                  3
M.mari C7WT       IQICSDDDLSCTGTSDITIVTAGMARTGDMSRIDLMRENAKIIKNYAKKIANAGDTKIFM
M.jann WT         IYVESDENLRIIDESDVVIITSGVPRKEGMSRMDLAKTNAKIVGKYAKKIAEICDTKIFV
M.jann C7like     IYVESDENLRIIDESDVVIITSGVPRKEGMSRMDLAKTNAKIVGNYAKKIAEICDTKIFV
M.jann C7likeGP   IYVESDENLRIIDESDVVIITSGVARKEGMSRMDLAKTNAKIVGNYAKKIAEICDTKIFV
                            70        *         *         *         *         *

                                 4 16 5
M.mari C7WT       ISNPVDMMTYKAFIESGYEKNQVFGLGTHLDSMRFKVAVAKYFEVHIDDVRTRIVGEHGD
M.jann WT         ITNPVDVMTYKALVDSKFERNQVFGLGTHLDSLRFKVAIAKFFGVHIDEVRTRIIGEHGD
M.jann C7like     ITNPVDVMTYKALVESKFEKNQVFGLGTHLDSLRFKVAIAKFFGVHIDEVRTRIIGEHGD
M.jann C7likeGP   ITNPVDVMTYKALVESGFEKNQVFGLGTHLDSLRFKVAIAKFFGVHIDEVRTRIIGEHGD
                            130       *         *         *         *         *

                                      6                 17 7 8   9
M.mari C7WT       SMVPLISATAVGGIPIVRLPKYENFPYDRILEKIKGYGKEIIDLKNGSEYGPASAIVNIV
M.jann WT         SMVPLLSATSIGGIPIQKFERFKELPIDEIIEDVKTKGEQIIRLKGGSEFGPAAAILNVV
M.jann C7like     SMVPLLSATSIGGIPIQRFERFKELPIDEIIEDVKTYGKQIIDLKGGSEFGPAAAILNVV
M.jann C7likeGP   SMVPLLSATSIGGIPIQRFERFKELPIDEIIEDVKGYGKQIIDLKGGSEFGPAAAILNVV
                            190       *         *         *         *         *

M.mari C7WT       RCIAHDEKRLLTLSAYIEDE
M.jann WT         RCIVNNEKRLLTLSAYVDGE
M.jann C7like     RCIVNNEKRLLTLSAYVDGE
M.jann C7likeGP   RCIVNNEKRLLTLSAYVDGE
                            250       *

                                 18          10
M.mari C7WT       IEGIKGGSCIGVPVKVGKNG
M.jann WT         FDGIR-DVCIGVPVKIGRDG
M.jann C7like     FDGIR-DVCIGVPVKIGKDG
M.jann C7likeGP   FDGIR-GVCIGVPVKIGKDG
                            270       *

                                 11    19
M.mari C7WT       IEEVIHMKMNDDEIEGFKKS
M.jann WT         IEEVVSIELDKDEIIAFRKS
M.jann C7like     IEEVVSIELNKDEIIAFRKS
M.jann C7likeGP   IEEVVSIELNKDEIIGFRKS
                            250       *

                               12
M.mari C7WT       FDLVKGYCKEIESI
M.jann WT         AEIIKKYCEEVKNL
M.jann C7like     AEIIKGYCEEVKNL
M.jann C7likeGP   AEIIKGYCEEVKNL
                            310
```

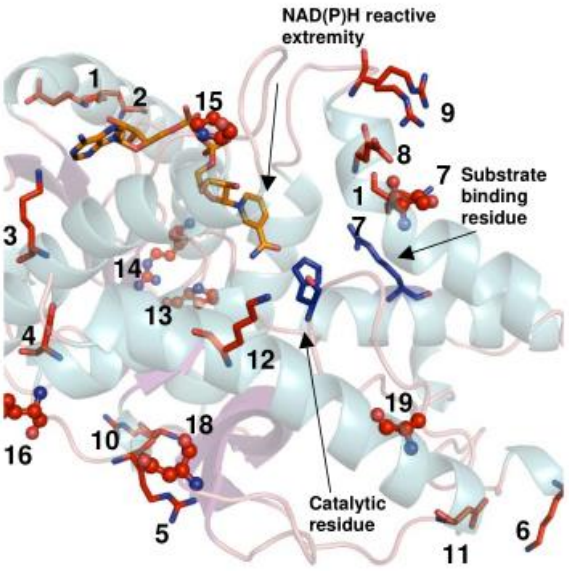

Fig. 6. Multiple alignment of Wt *M. jann*, Wt *M. mari* C7, and *M. jann* C7 like and C7GP like mutants. The multiple alignment shows the 19 amino acids of the Wt *M. mari* C7 (green, first sequence) that have been introduced into the Wt *M. jann* MalDH sequence at equivalent positions (red, second sequence). The *M. jann* C7 like mutant corresponds to the Wt *M. jann* MalDH with 12 of the19 targeted amino acids

present in *M. mari* C7 added (1 to 12 in green, third sequence). The M. jann C7 like GP mutant contained the full set of targeted amino acids present in Wt *M. mari* C7 (1 to 19 in green, fourth sequence). The linear numbering of amino acids is shown below the alignment.

The small inset shows the location of mutations on the *M. jann* MalDH structure of the monomer (PDB accession number,1HYG). α–helices, β-strands and loops are in blue, purple and pale orange, respectively. The first set of mutated amino acids is represented in red stick, the second is in small red balls. The numbering refers to their location indicated on the sequence alignment. The catalytic histidine (H178) and the substrate binding residue (R154) are shown in blue sticks. The coenzyme reactive extremity (orange stick) is indicated.

We carefully inspected the *M. jann* MalDH structure as a guide to discriminate between substitutions that preferentially target intra-monomeric salt bridges rather than those located at interfaces that contribute to tetramerization. The first mutant, *M. jann* C7 MalDH, contained 12 substitutions that target the salt bridges, while the second mutant, *M. Jann* C7GP, contained seven additional substitutions (i. e, five glycine were added and two proline residues removed) located in loops, which connect β-strands and α-helices. In both mutants, the targeted residues were substituted by the amino acids found in *M. mari* C7 at the same position (Fig. 6). The position of the substitutions is shown on the structure of the Wt *M. jann* MalDH monomer (Fig. 6). Recall that none of these amino acids participate to substrate-binding or catalytic reaction.

The resulting *M. jann* C7 and *M. jann* C7GP MalDHs, were purified and their temperature-dependent activity profiles were recorded. As previously noted, the Wt *M. jann* MalDH has the typical profile of a hyperthermophilic enzyme with an A-T_{opt} close to 90°C. The activity profile of *M. jann* C7 MalDH is strongly shifted towards lower temperatures with an A-T_{opt} value of 65°C (Fig. 7A). Our data showed that disruption of intra-monomer ionic interactions could be one of the mechanisms that drove adaptation toward mesophily in *Methanococcales*.

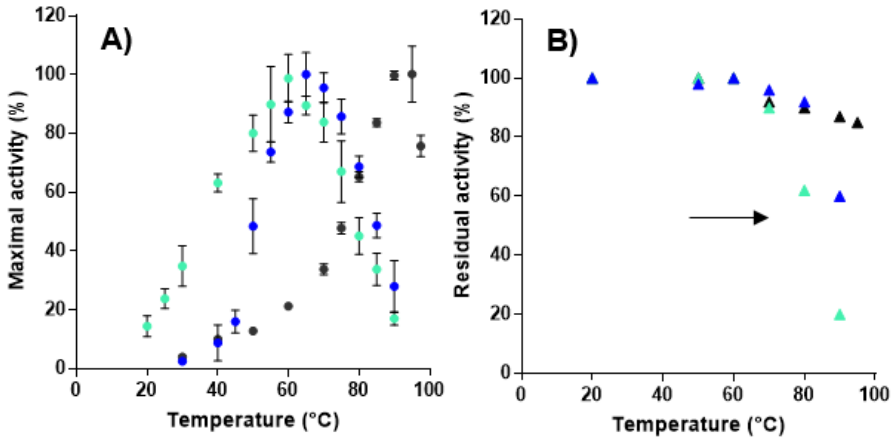

Fig 7. Effects of mesophilic-like mutations on *M. jann* MalDH. (A) Temperature-dependent activity profile of Wt *M. jann* MalDH, black circles. *M. jann* C7 MalDH mutant, dark blue circles. *M. jann* C7GP MalDH mutant, cyan circles. The averaged values are expressed as % of activity relative to the maximal value recorded for each enzyme. For a given MalDH, optimal temperature for activity (A-T_{opt}) corresponds to the peak of the curve, i.e., the maximal value recorded. Error bars are shown. **(B)** Thermostability probed by residual activity measurement. Wt *M. jann* MalDH is in black triangles, *M. jann* C7 MalDH in dark blue triangles and *M. jann* C7GP MalDH in cyan triangles. The arrow indicates $T_{M1/2}$ values.

For the *M. jann* C7GP MalDH, the resulting behavior was different. The A-T_{opt} has a value of 60°C, indicating that modifying the G and P content did not have a major effect on this parameter compared to *M. jann* C7. However, the profile of *M. jann* C7GP MalDH showed that the relative maximum activity below A-T_{opt} (20-60°C range) was significantly increased compared to the *M. jann* C7 enzyme (Fig. 7A). Without data based on the Wt *M. mari* MalDH, a comparison with its activity profiles was not possible. We also recorded the apparent conformational stability using residual activity measurements. The data showed that the two sets of mutations affected the thermal stability by shifting the $T_{M1/2}$ towards lower temperature compared to the Wt *M. jann* MalDH. However, $T_{M1/2}$ of 83°C and 90°C indicated that the mutants still behave as hyper thermostable scaffolds (Fig. 7B). We noted that the characterization of the adenylate kinase from *M. mari* reports an excellent activity over a moderate temperature range and a high thermal conformational stability (Davlieva and Shamoo 2010).

7) Conformational stability of ancestral and present-day *Methanococcales* MalDHs under γ-irradiation oxidation by •OH and $Cl_2^{\bullet-}$ free radicals.

To test whether high conformational thermal stability favours the capacity to resist unfolding under strong γ-irradiation-induced oxidation, we monitored the circular dichroism (CD) spectrum at 25°C of a set of present-day *Methanococcales* MalDHs (*M.infe* and *M. jann* (both OGTs = 85°C), and *M. form* (OGT = 75°C)), and their deepest ancestors (LMCA/A35 ($estOGT_{MalDH}$ = 84°C), *Methanocaldococcaceae*/A34 ($estOGT_{MalDH}$ = 87°C) and *Methanococcaceae*/A19 ($estOGT_{MalDH}$ = 73°C)) before and after exposure to a ^{60}Cobalt source in oxidizing conditions (Fig. 8A). The LDH from *S. rumi* (OGT = 37°C) and the MalDH from *M. kand* (OGT = 98°C) were also tested (Fig. 8B). In the irradiation conditions, the medium is strongly oxidising as the reducing free radicals are scavenged. For the set of *Methanococcales*, the comparison showed no significant differences between the irradiated and non-irradiated enzymes (Fig. 8A). This was also the case for MalDH from the hyperthermophilic archaea *M. kand* (Fig. 8B). On the other hand, for the *S. rumi* enzyme, the CD spectrum obtained after irradiation showed strong modifications: the value of the molar ellipticity at 222 nm increased, the lowest intensity peak was shifted to 208 nm, the zero value of the molar ellipticity at 200 nm was shifted, and the positive signal disappeared, showing a transition towards a less structured and less compact state (see arrows in Fig. 8B).

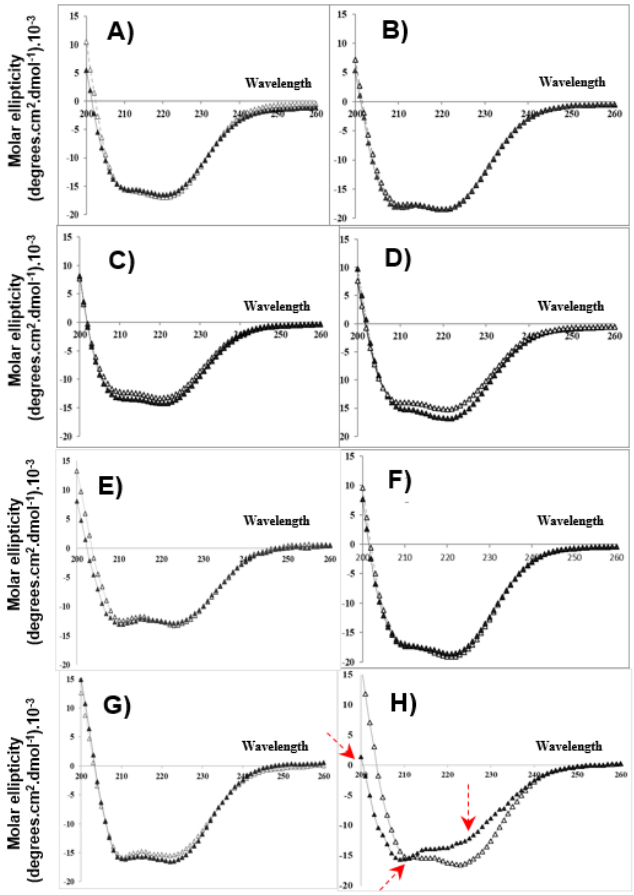

Fig. 8. Effect of γ-irradiation on the circular dichroism spectra of ancestral and present-day *Methanococcales* MalDHs. Open and closed triangles correspond to CD spectra taken before and after irradiation. MalDH from **(A)** *M. infe* (OGT = 85°C), **(B)** *M. jann* (OGT = 85°C), **(C)** *M. form* (OGT = 75°C), **(D)** LMCA/A35 ($estOGT_{MalDH}$ = 84°C), **(E)** *Methanocaldococcaceae*/A34 ($estOGT_{MalDH}$ = 87°C), **(F)** *Methanococcaceae*/A19 ($estOGT_{MalDH}$ = 73°C), **(G)** *M. kand* (OGT = 98°C, outgroup), and **(H)** the LDH from *S. rumi* (OGT = 37°C). To the exception of the *S. rumi* enzyme, for which the applied dose was 1,500 Gy, the other enzymes received (in average) a dose of 4,000 Gy.

The modification of UV-visible spectra of a protein after γ-irradiation is a strong indicator of protein residue oxidized (Houee-Levin and Bobrowski 2013). Accordingly, we checked whether methanococcales MalDHs were subjected to attack by reactive species by recording their UV-visible spectra before and after irradiation. A set of two ancestral (LMCA/A35 and *Methanococcaceae*/A19) and two present-day *Methanococcales* MalDHs (*M. jann* and *M. form*) were tested (Fig. 9).

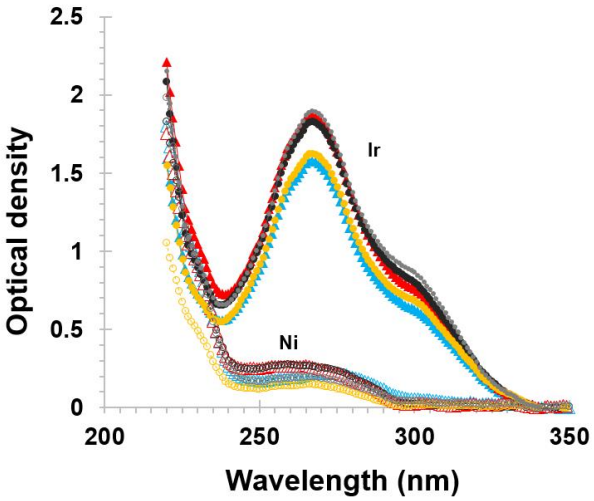

Fig. 9. Effect of γ-irradiation on the UV-visible spectra of some ancestral and present-day methanococcales MalDHs. Ni: non-irradiated, open symbols, Ir : irradiated, closed symbols. Ancestral MalDHs : LMCA/A35 ($estOGT_{MalDH}$ = 84°C), red triangles; *Methanococcaceae*/A19 ($estOGT_{MalDH}$ = 73°C), blue triangles. Present-day MalDHs: *M. form* (OGT = 75°C), orange circles; *M. jann* (OGT = 85°C), black circles; *M. infe* (OGT = 85°C), grey circles.

The data clearly showed that chemical modifications occurred after irradiation. We concluded that even if OH-$Cl_2^{\bullet-}$ radicals have oxidized numerous amino acids this was not sufficient to unfold the hyperthermostable MalDHs, suggesting that strong stabilizing interactions are still efficient in the tetrameric scaffold. Due to the limited amount of N_2O in the samples to be irradiated, further investigations at higher doses were difficult to perform. However, we tried to test the conformational stability of the most ancestral enzyme at doses of 7,200 and 10,500 Gy by recording the CD spectra. The data showed that these doses have a small effect on the CD spectrum of the LMCA/A35 suggesting that only a small fraction of the molecules begin to unfold (Fig. 10A). As previously, further drastic treatments are necessary to induce unfolding, even if the enzyme has been subjected to oxidation (Fig. 10B). The thermal treatment applied to the irradiated enzyme produces an intermediate state that is different from the typical unfolded state obtained after acidification of the sample.

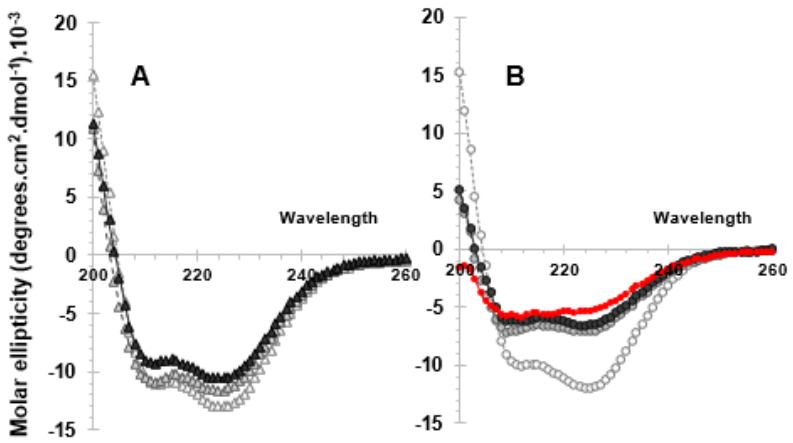

Fig. 10. Effect of high irradiation doses on LMCA/A35 MalDH. **(A)** CD spectra taken before (Open triangles) and after irradiation at 7,200 Gy (Gray triangles) and 10,500 Gy (Dark triangles). **(B)** CD spectra after adding thermal treatment and acidification to samples used in A. 0 Gy (Open circles), 7,200 Gy (Gray circles),10,500 Gy (Dark circles) and 10,500 Gy+ HCl (red circles).

8) Quantification of γ-irradiation oxidative damages.

Native mass spectrometry was used to characterize the extent of protein damage after irradiation. This method allows the observation of the oligomeric state (homotetramer) of the protein under study and its molecular mass to be monitored simultaneously. Some of the mass spectrometry spectra are shown as Supplementary Fig. S7. They showed that the enzymes remained tetrameric after irradiation. We observed also that, after irradiation, chemical modifications by reactive species induced an increase in the molecular mass of each MalDH at the dose administered (Fig. 11, Supplementary Table S3). We observed that LMCA/A35, and *M. kand* MalDHs accumulated a higher number of modifications than the other enzymes. At this stage, it was not possible to determine the reasons for this, even it can be assumed that differences in the amino acid sequence may lead to different reactivity with oxidative species. As the SEC was not efficient enough to remove salts, knowing that the KCl concentration was of 0.4 M, the peaks of the tetramers are large and the calculated molecular weight is overestimated. For this reason, we also performed reversed phase chromatography to obtain more reliable mass increases. Under these conditions, the mass increases were lower than under native conditions. However, at very high irradiation doses, the chemical modifications were so numerous that it was sometimes impossible to measure a molecular weight.

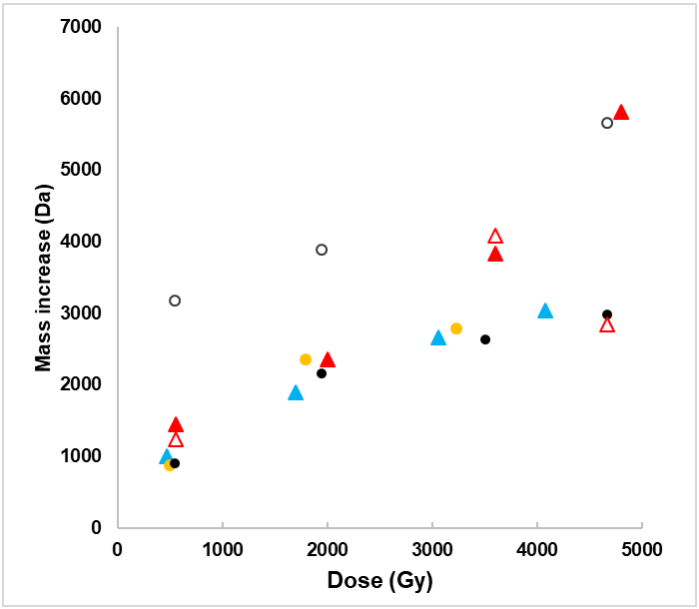

Fig. 11. Effect of irradiation doses on molecular mass of some ancestral and present-day MalDHs. The molecular mass changes detected by mass spectrometry are expressed in Dalton for each enzyme investigated. Ancestral MalDHs: LMCA/A35 ($estOGT_{MalDH}$ = 84°C), red triangles, *Methanococcaceae*/A19 ($estOGT_{MalDH}$ = 73°C), blue triangles. Modern MalDHs: *M. form* (OGT = 75°C), orange circles, *M. jann* (OGT = 85°C), black circles, *M. kand* (OGT = 98°C, outgroup), open circles.

9) Effect of γ-irradiation induced oxidation on MalDH enzymatic activity.

We then investigated the effect of irradiation on the enzymatic capacity of some ancestral and extant MalDHs from *Methanococcales* (Fig. 12). After irradiation, all samples were stored at 25°C prior to enzymatic assay. All assays were performed at 70°C, with the exception of Methanococcaceae/A19 and *S. rumi* LDH for which the temperature was 60°C. With *S. rumi* LDH, taken as a mesophilic example, the data showed it was strongly deactivated with a maximum activity value of 10% after irradiation at 420 Gy. The ancestral and modern methanococcales MalDHs shared a common tendency to deactivate as the irradiation dose increased. The MalDH Methanococcaceae/A19 completely lost its activity at 4,080 Gy, suggesting that it was the most sensitive ancestral MalDH in *Methanococcales*. The data did not allow us to distinguish between two possible explanations for the deactivation. In the first one, only a fraction of the enzymes was inactivated, the rest being able to maintain full activity. In the second, the activities of all the enzyme molecules are modified (without loss of structure, as previously monitored by CD), so that their enzymatic parameters (maximum rate and/or affinities for substrate and coenzyme)

were altered in a way that reduces their efficiency. The more oxidized the residues, the less effective the enzymes. Since the reactive species are produced homogeneously in solution during irradiation, the second scenario was the most likely. We decided to incubate the irradiated and non-irradiated enzymes at 90°C for 15 min and monitor the activity again to explore the effect of an additional physicochemical stress (Fig. 12B). The data showed that the ancestor of *Methanococcaceae*/A19 was completely inactivated, whereas the other MalDHs retained a low enzymatic capacity. It is therefore reasonable to assume that incubation at high temperature selected for a population of conformers with reduced enzymatic capacity.

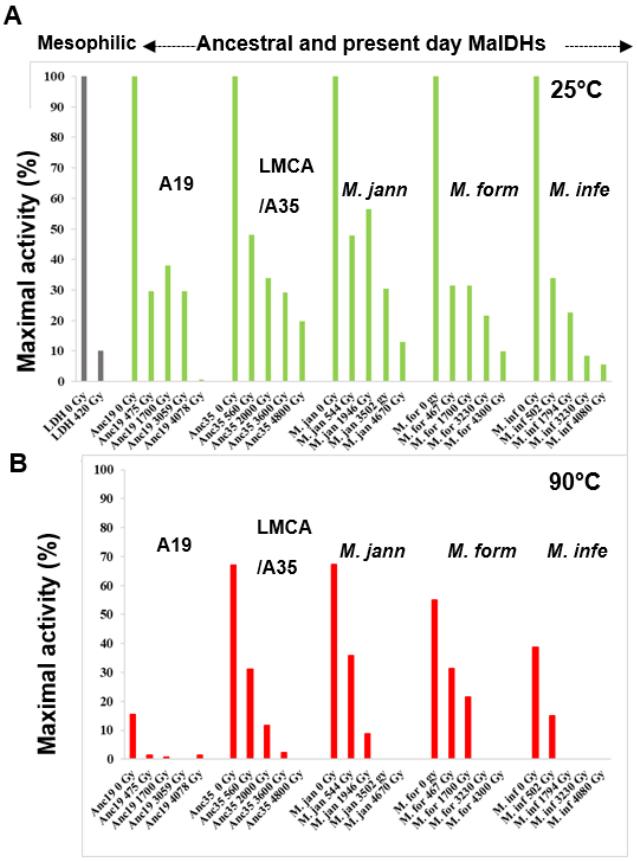

Fig.12. Effect of γ-irradiation dose on enzymatic activity. LMCA/A35 ($estOGT_{MalDH}$ = 84°C), *Methanococcaceae*/A19 ($estOGT_{MalDH}$ = 73°C), *M. form* (OGT = 75°C), *M. jann* (OGT = 85°C), *M. infe* (OGT = 85°C). **(A)** Changes in enzymatic activity (using OAA as substrate) of different methanococcales MalDHs after exposure to different doses of γ-irradiation. *S. rumi* LDH (using pyruvate as substrate) was used to illustrate the behavior of an enzyme from a mesophile. The results are expressed as % of the enzymatic activity recorded before irradiation (0 Gy) for each enzyme. **(B)** Effect of an additional incubation at 90°C on irradiated and non-irradiated samples.

In the case of the MalDH from the ancestor of *Methanococcaceae*/A19 (OGT = 67°C), which has an A-T_{opt} of 60°C, the amplitude of the effect was maximal, whereas for the other enzymes, which have an A-T_{opt} greater than 80°C, the effect was reduced. When the enzymes were modified by irradiation, the effect of thermal treatment on the population of the conformers with lower activity was enhanced. Consequently, at high doses, all enzymes were inactive after thermal treatment. Our protocol confirmed that the ancestor of *Methanococcaceae*/A19 behaves differently from enzymes with hyperthermophilic properties.

In a previous study using LDHs from organisms with different OGTs, it was observed that none of the amino acids involved in catalysis were damaged by oxidation after irradiation, although the enzymes were inactive (Halgand, et al. 2020). It was proposed that this phenomenon is based on the ability to maintain LDHs in a conformational state unproductive for catalysis (Halgand, et al. 2020). We tried to apply the same experimental strategy to the different MalDHs analyzed here. Unfortunately, we were unable to find efficient conditions to induce limited proteolysis on the irradiated sample, which prevented the use of mass spectrometry on the various fragments obtained by this method and thus the identification of the amino acids affected by reactive species.

10) Thermal and irradiation stresses alter the substrate-binding affinity of MalDHs.

Several works have shown that the loss of enzymatic activity during thermal or chemical unfolding precedes large conformational changes (Yao, et al. 1984; Xie and Tsou 1987; Zhang, et al. 1993). Later, using a set of eight enzymes, the mechanism by which they lose activity as temperature rises was analyzed, leading to the conceptualization of the equilibrium model (reviewed in (Daniel and Danson 2013)). The model states that the transition from the folded to the unfolded state, proceeds through an intermediate folded state, which can sample two (active or inactive) catalytic site conformational sub states. Due to their intrinsic dynamical properties, temperature-driven activity shifts of enzymes could be therefore the consequence of (i) catalytic site reorganizations that affect the pKa of amino acids involved in catalysis, (ii) the maximal velocity rate or (ii) modifications in the substrate-binding affinity. Our findings are consistent with this model. Indeed, we have shown that the loss of MalDH activity was not necessarily associated with unfolding. This was clearly the case for the MalDH of the *Methanococcaceae*/A19 ancestor, which loses activity at temperatures above 60°C, while remaining

folded. This was also the case for all MalDHs after irradiation. In order to understand the mechanisms of inactivation, we recorded the kinetic parameters of three hyperthermophilic MalDHs (*M.jann, M.infe*, and *M. form*) at 75°C and the *Methanococcaceae*/A19 ancestor at 60°C (Table 2).

Table 2. Kinetic parameters of MalDH from present-day *Methanococcales* (*M. jann*, *M. infe*, and *M.form*), the ancestors of *Methanococcales* (LMCA/A35), *Methanocaldococcaceae* (A34) and *Methanococcaceae* (A19).

Taxa	Experimental temperatures	"Stress"	K_m (mM)	k_{cat} (s^{-1})	k_{cat}/K_m ($M^{-1}.s^{-1}$)
M. infe	75°C		0.9	1,150	$1.3\ 10^6$
M. jann	75°C		1.1	1,031	$0.9\ 10^6$
M. form	75°C		0.8	1,189	$1.4\ 10^6$
Methanococcaceae (A19) ancestor	60°C		0.6	1,143	$1.9\ 10^6$
	75°C	Higher than A-T_{opt}	7.7	686	$8.9\ 10^4$
Methanococcales ancestor (A35)	75°C		0.3	960	$3.2\ 10^6$
	75°C	Irradiation at 2,000 Gy	2.9	732	$2.5\ 10^5$
Methanocaldococcaceae (A34) ancestor	75°C		1.0	915	$0.9\ 10^6$

Under these conditions, k_{cat} values between 915 and 1189 s^{-1} were quite similar for all enzymes and close to typical values for MalDHs (Shimozawa, et al. 2022). Phylogenetic analyses have shown that methanococcales MalDHs belong to an intermediate group of enzymes between the clade of tetrameric MalDH type 3 and LDH (Brochier-Armanet and Madern 2021). Present day and ancestral methanococcales MalDHs have Km values for OAA in the range of 0.3 to 1.1 mM, indicating a lower affinity than that of MalDH type 3 (Brochier-Armanet and Madern 2021), an observation that was previously reported for another hyperthermophilic MalDH from the intermediate group (Roche, et al. 2019). A detailed description of this phenomenon required the acquisition of structural information on the respective enzymes used in this study, work that is currently underway.

We then recorded parameters using *Methanococcaceae*/A19 MalDH at 75°C, a temperature higher than its A-T_{opt}. We also analyzed the effects of an irradiation dose of 2,000 Gy, using LMCA/A35 MalDH as the target enzyme. The data showed that these two enzymes became less efficient, as indicated by their k_{cat}/K_m values, which fall well below the values recorded at A-T_{opt}. This was mainly because their K_m values for OAA increased strongly (Table 2). This might indicate that their respective substrate binding

site was in an unfavorable configuration to accommodate OAA. A previous work on an hyperthermophilic LDH showed that irradiation-induced inactivation maintains the enzyme in a low-affinity pyruvate-binding state, preventing the enzyme from accessing its competent state for catalysis (Halgand, et al. 2020).

Discussion

One of the aims of this study was to experimentally investigate the process of enzyme thermoadaptation using *Methanococcales* MalDH as model. The inference of OGT along the *Methanococcales* phylogeny using present-day MalDH sequences is consistent with the seminal work performed on complete proteomes by Lecocq et al. (2021), indicating that the thermoadaptation was so strong that it is still detectable today at the level of a single protein. Specifically, we showed that (i) the LMCA lived in a hot environment and (ii) some of its descendants evolved to colonize cooler environmental niches. We then sought to determine whether there was a good correlation between the thermal properties of the MalDH model enzyme and the OGT of ancestral and extant *Methanococcales*. We found that the ancestral MalDH in *Methanococcales* was both a hyperthermostable and thermoactive enzyme, confirming the hot origin of this archaeal order. We also observed that although numerous amino acid substitutions have accumulated in the sequences of present-day MalDH since the LMCA, their effects have been buffered to maintain the original phenotype. We observed that the first step in the evolutionary process leading to the mesophilic lineages was different. In fact, the MalDH inferred in the *Methanococcaceae*/A19 ancestor showed a maximal activity at moderate temperature without compromising its high thermal stability. Furthermore, the A-T_{opt} value of this enzyme (60°C) is close to the estOGT_{MalDH} of the *Methanococcaceae*/A19 ancestor (73°C). This correlation shows that monitoring the A-T_{opt} of enzymes may be more reliable than monitoring their conformational stability. The behavior of the *Methanococcaceae*/A19 ancestor MalDH is consistent with the microstate ensemble model of protein structure. This model proposes that temperature samples a set of conformational sub-states that are structurally close to the native state, but for which the catalytic efficiency and substrate binding capacity are different (Wrabl, et al. 2011). Molecular dynamics simulations have shown that the onset of the activity drop, which can occur well below the melting temperature, is determined by the activation energy between the productive and unproductive conformers (Maffucci, et al. 2020). Consequently, any shifts in catalytic activation energy induced by mutations will alter the balance between these states,

allowing thermal adaptation to proceed (Dong, et al. 2018; Fusco, et al. 2022; Koenekoop and Aqvist 2023).

Here, the substitutions selected in the ancestral MalDH of *Methanococcaceae*/A19 have most likely lowered the energy barriers to access catalytically competent conformers without the need for high thermal energy, allowing for a rapid and efficient adaptive response. The characterization of this MalDH also allowed us to propose that incompetent conformers sampled at high temperature exhibit local perturbations within their catalytic site, which reduce substrate binding efficiency. In the context of these observations, the introduction of mesophilic-like mutations, using a MalDH from a modern hyperthermophile as a scaffold, shifts the A-T_{opt} towards low temperatures with a limited effect on thermal stability. Our work illustrates that the thermal adaptation of enzymes is much more complex than a uniform shift in the melting and optimum activity temperatures. Structural and dynamic studies are being carried out on several of the enzymes used in this work to go further in the understanding of thermal adaptation process. We also investigated the relationship between high thermal stability and a putative ability to resist γ–irradiation induced unfolding. We found that the MalDH inferred in the LMCA/A35 ancestor is a polyextremophilic enzyme capable of withstanding both strong thermal and radiative stress. In a previous study, we proposed that resistance to γ-irradiation might be an indirect consequence of the overall stability of the proteins rather than a specific adaptation (Halgand, et al. 2020). Consistent with the present work, it is reasonable to propose that adaptation to elevated temperature is mediated by increased stability of the protein, which may also favor resistance to γ-irradiation. Further studies are needed to gain insight into this phenomenon. The ability to resist to γ–irradiation induced unfolding has been retained (but hidden) in modern hyperthermophilic enzymes, mainly because of the strong selective pressure continuously exerted by environmental temperature.

Materials and Methods

Phylogenetic analyses and ancestral MalDH sequence reconstruction

MalDH protein sequences were retrieved from the *nr* protein sequence database at the NCBI. The dataset encompassed MalDH sequences from ten *Methanococcaceae*: *Methanococcus maripaludis* C5 (YP_001097480), *Methanococcus maripaludis* C6 (YP_001548297.1), *Methanococcus maripaludis* C7 (YP_001330878.1), *Methanococcus maripaludis* S2 (NP_987765.1), *Methanococcus maripaludis* X1 (YP_004742269.1), *Methanococcus vannielii* SB (YP_001324052.1), *Methanococcus voltae* A3

(YP_003707533.1), *Methanothermococcus thermolithotrophicus* (WP_018154699.1), *Methanococcus aeolicus* Nankai-3 (YP_001324807.1), and *Methanothermococcus okinawensis* IH1 (YP_004576638.1), and eight *Methanocaldococcaceae*: *Methanotorris formicicus* (WP_007044377.1), *Methanotorris igneus* Kol5 (YP_004483657.1), *Methanocaldococcus fervens* AG86 (YP_003128040.1), *Methanocaldococcus jannaschii* DSM 2661 (NP_247466.1), *Methanocaldococcus* sp. FS406-22 (YP_003459168.1), *Methanocaldococcus vulcanius* M7 (YP_003246708.1), *Methanocaldococcus villosus* (WP_004592381.1), and *Methanocaldococcus infernus* ME (YP_003616626.1), and seven sequences from other *Methanomada* lineages: six *Methanobacteriales* (*Methanobacterium* sp. AL-21 (YP_004289802.1), *Methanobacterium* sp. SWAN-1 (YP_004520598.1), *Methanothermobacter marburgensis* str. Marburg (YP_003849548.1), *Methanothermobacter thermautotrophicus* str. Delta H (NP_275331.1), *Methanobrevibacter ruminantium* M1 (YP_003423997.1), *Methanosphaera stadtmanae* DSM 3091 (YP_447713.1)), and one member of *Methanopyrales* (*Methanopyrus kandleri* AV19 (NP_614352.1)). Sequences were aligned using MAFFT v7.505 with the accurate option L-INSI (Katoh and Standley 2013). A maximum likelihood phylogeny was inferred using PhyML with the LG model, a gamma distribution to consider across site rate variations (four discrete categories), as suggested by ModelFinder implemented in IQ-TREE (version 2.3.4) according to the Bayesian Information Criterion (Nguyen, et al. 2015; Kalyaanamoorthy, et al. 2017), and the NNI+SPR option to optimize the tree topology. The length of the branches of the resulting tree was optimized using BPPML with the branch heterogeneous model COALA, assuming the non-stationarity of the evolutionary process, and with a gamma distribution to model the heterogeneity of evolutionary rates among sites (Dutheil and Boussau 2008; Groussin, et al. 2013). At each node of the *Methanococcales* phylogeny, ancestral sequences were reconstructed using BPPANCESTOR (Dutheil and Boussau 2008), with the evolutionary parameters estimated with BPPML and the optimized ML tree as input. For details regarding the parameters used for BPPML and BBPancestor (see Supplementary Table S4). As most ASR methods, BPPANCESTOR ignores gaps. However, MalDH sequences of *Methanococcales* contains only two one aa-gaps, at positions 262 and 267. The first one corresponds to a deletion found only in *Methanocaldococcus villosus* and *Methanocaldococcus infernus*, while the second is shared by *Methanococcus maripaludis*, *Methanococcus vannielli*, *Methanococcus voltae*, and *Methanothermococcus thermolithotrophicus*. Since the number of gaps in the sequences is small and their positioning in the alignment is clear, we expect that they should not have a major impact ASR. The

multiple alignment of present-day MalDH, the ML tree file, and ancestral MalDH sequences are provided as online supplementary material.

Estimation of present-day and ancestral OGT

We performed a correspondence analysis (CA) of the amino acid content of the MalDH sequences using the R libraries ADE4, APE and NLME (Dray and Dufour 2007; Paradis and Schliep 2019; Pinheiro and Bates 2024). Note that we did not consider tryptophan (W) because almost all MalDH protein sequences lack this amino acid, with the exception of MalDH from *M. okin* IH1, *M. volt* A3, and *M. aeol* Nankai-3, which contain a single tryptophan. Pearson's product-moment correlation were computed with ADE4.

To build the molecular thermometer, we used four linear models: the standard linear model (SLM), and models by Martins and Hansen (MAM) (Martins and Hansen 1997), by Grafen (GRM) (Grafen 1989), and by Felsenstein (FBM) (Felsenstein 1985), the three latter accounting for phylogenetic relationships (Paradis and Schliep 2019). The models were used to correlate the scores of the MalDH protein sequences on the first axis of the CA with the OGT of the present-day Methanococcales strains. For MAM, FBM, and GRM models, we used the ML tree of the MalDH as input.

The intercept and slope coefficients of the regression were: 63.45098 and -195.4594 (SLM); 62.48197 and -182.24615 (MAM); 63.17399 and -173.70077 (GRM); 62.3114 and -71.0827 (FBM). The reliability of the models was tested by predicting OGT of the 17 methanococcales strains for which OGT are known. They were then used to predict ancestral OGT at each node of the *Methanococcales* phylogeny using the inferred ancestral MalDH protein sequences. OGTs were also predicted applying the standard linear model on the content of amino acids I, V, Y, R, E and L highlighted by Zeldovich et al (2007).

Gene synthesis and protein expression and purification.

All the ancestral and present day MalDH gene sequences studied in this work were subjected to codon optimization for over expression in *Escherichia coli.* The genes have been synthesized by the Genecust company. In the case of the two *M. jann* MalDH mutants, an extension of six histidine (His tag) was fused to their C-terminus in order to facilitate the purification using affinity chromatography. The other genes were synthesized without any extension.

All the genes were sub-cloned into the pet 20a vector between the *NdeI* and *BamHI* restriction sites. The constructs were transformed into BL21(DE3) plysS cells and selected on LB-agar plate containing

100 μg ml-1 ampicilin. A single colony was cultured overnight at 37°C in 100 ml LB medium containing 100 μg ml-1 ampicilin. 25 ml of this culture were transferred into 1L of LB medium containing 100 μg ml-1 ampicilin. The cells were grown at 37°C until an OD 600 of 0.6 was reached. The temperature was quickly lowered to 4°C and the cells were kept on ice for three hours, then IPTG was added at a final concentration of 0.2 mM to induce expression, which was continued overnight at 20°C. The bacterial cells were then harvested by centrifugation. The pellets were suspended in 50 mM Tris-HCl pH 7, 50 mM NaCl (Buffer A) and frozen at -20.

After thawing of the cells, DNase at 5 μg ml-1 was added to the suspension. The cell suspension was sonicated with a Branson sonicator at 25% intensity during three cycles of 1 min. The extract was centrifuged at 18,000 g for 30 min at 4°C. The supernatant was filtered on a 0.45 μm (Amicon). With the two His-tagged mutants, the extract was passed through a 5mL HisTrap Q HP column (GE Healthcare Life Science). The column was washed with 20 mL of 50 mM Tris-HCl pH7, 200 mM NaCl and by 25 mL of 20 mM imidazole pH 7, 200 mM NaCl. Then, the two *M. jann* MalDH mutants were eluted with 300 mM imidazole pH 7, 50 mM NaCl. The resulting enzyme preparation was concentrated and dialyzed in Buffer A using Amicon Ultra-30 concentrators. The enzyme was then loaded on an anion exchange Uno Q (BioRad) and eluted with a linear gradient from 0 to 1M NaCl buffered by 50 mM Tris-HCl pH7. The active fractions were pooled, concentrated and loaded on a size exclusion chromatography column (SEC) equilibrated with buffer A. An Enrich 650 (Biorad) column was used.

With all the other enzymes without His-tag extension, the crude extract obtained after sonication was incubated 15 min at 70°C and centrifugated at 18,000 g for 30 min at 4°C. The supernatant was filtered on a 0.45 μm (Amicon). The clear supernatant was loaded on a Q sepharose (2x5cm) and eluted using a linear gradient of gradient from 0 to 1M NaCl in buffer A. The active fractions were pooled, concentrated and loaded on the SEC equilibrated with buffer A. Fractions containing the enzymes under study were concentrated and stored at -80°C in buffer A with 20% glycerol. In the case of *M. kand* MalDH the SEC was equilibrated with 0.4 M KCl, Tris-HCl 50 mM pH7 (Brochier-Armanet and Madern 2021).

Protein irradiation

The proteins were dissolved to a final concentration of 0.3 mg/mL (2.4 μM) in 50 mM Tris-HCl pH 7+KCl 0.4M. They were irradiated in N_2O atmosphere in the panoramic ^{60}Co γ-source IL60PL (Cis-Bio International (France)) at the University Paris-Saclay (Orsay, France). The absorbed dose was

determined by Fricke dosimetry (Spinks and Woods 1990). The doses were comprised between 500 and 10,000 Gy, delivered with a dose rate up to 31.8 Gy/min.

Interaction of ionizing radiations with water leads to the formation of free radicals following equation 1:

$H_2O \rightarrow {}^{\bullet}OH, H^{\bullet}, e^-_{aq}, H_2, H_2O_2, H^+, OH^-$ (1)

In N_2O atmosphere, e^-_{aq} is scavenged leading to the formation of OH radicals according to equation (2)).

in the presence of Tris buffer and KCl and in an atmosphere of N2O, the following reactions take place:

$e^-_{aq} + N_2O \rightarrow OH^{\bullet} + OH^- + N_2$ (2) (Spinks and Woods 1990)

Tris + $^{\bullet}OH \rightarrow$ Tris•(-H) + H_2O (4) (Hicks and Gebicki 2001), $k_3 = 1.5\ 10^9\ mol^{-1}\ L\ s^{-1}$ (3)

$Cl^- + {}^{\bullet}OH \rightleftharpoons ClOH^{\bullet}$; $k_4 = 4.3 \times 10^9\ mol^{-1} L\ s^{-1}$; $k_{-4} = 4.3 \times 10^9\ mol^{-1} L\ s^{-1}$ (4)

$ClOH^{\bullet-} + H^{+\cdot} \rightleftharpoons HClOH^{\bullet}$ $k_5 = 3 \times 10^{10}\ mol^{-1} L\ s^{-1}$; $k_{-5} = 1.0 \times 10^8\ s^{-1}$ (5)

$HClOH^{\bullet} \rightleftharpoons Cl^{\bullet} + H_2O$ $k_5 = 5 \times 10^4\ s^{-1}$; $k_{-5} = 2.5 \times 10^5\ s^{-1}$ (6)

$Cl^{\bullet} + Cl^{-\cdot} \rightleftharpoons Cl_2^{\bullet-}$ (7) $k_5 = 8.5 \times 10^9\ mol^{-1} L\ s^{-1}$; $k_{-5} = 6 \times 10^4\ s^{-1}$ (7)

Thanks to reaction (2) the yield of $^{\bullet}OH$ radicals is doubled: 0.54 µmol J^{-1}. The total amount of $^{\bullet}OH$ radicals is proportional to the dose, i.e., the total [•OH] delivered to the solution was between 0.27 mM and 5.4 mM. The H_2O_2 yield is lower (0.07 µmol J^{-1}). In the presence of Tris buffer and KCl, $^{\bullet}OH$ radicals can react either with the protein or with the Cl^- ions. Reaction (3) produces carbon-centered radicals that are reductants and usually poorly reactive toward proteins.

At pH around neutrality equilibria (4) to (7) are involved. As a consequence, a mixture of OH• - $Cl_2^{\bullet-}$ is created in the solution. Both are oxidizing free radicals, $Cl_2^{\bullet-}$ being less reactive than OH radicals (Valiev, et al. 2009).

Circular dichroism spectroscopy

CD spectra were recorded at 25°C, on a MOS 500 circular dichroism spectropolarimeter (BioLogic) using a quartz cuvette with a path-length of 0.1 cm. The spectra were recorded at 50 nm / min with a bandwidth of 2.0 nm and an integration time of 6 sec, over the wavelength range 190-260 nm.

Enzymatic assays

The standard assay was performed at 60°C when using Anc 19 MalDH and at 70°C with all the other enzymes used in this study, respectively. The standard assay mixture of 0.5 ml contained 0.2 mM NADH,

841 the various enzymes under study and 50 mM Tris-HCl pH 7. A 3 minutes pre –incubation period was
842 applied to the mixture. Then, the reaction was started by the addition of the oxaloacetate solution (0.8
843 mM final concentration) and the d*A*/d*t* was immediately followed during 120 sec by recording the
844 decrease of NADH absorbance (*A*) at 340 nm in a thermostated Jasco spectrophotometer.
845 To record the temperature-dependent enzymatic activity profile, the reaction mixture for each enzyme
846 was incubated at various temperature ranging from 25° to 95°C. The measurements were done in
847 triplicates. The data were expressed as a percentage of the maximal activity recorded for a given
848 enzyme.
849 To record the effect of irradiation on enzymatic activity, an aliquot of each enzyme was taken from the
850 various irradiated solutions. The data were expressed in % with respect to the activity recorded using
851 non-irradiated samples.
852 Our protocol allows comparing directly the effects of different treatments on activity.
853
854 **Size-exclusion chromatography (SEC) coupled to mass spectrometry (MS).**
855 SEC-MS coupling was set up using a TSK 3000 SW gel filtration column (Interchim, 1 x 300 mm). Elution
856 buffer was 100 mM ammonium acetate, pH 7, infused at 0.02 ml/min flow rate and directly injected in
857 the electrospray ionization source. Ten µl of standard and irradiated protein solution initially at 90 µM
858 concentration were loaded on the SEC column. Mass spectrometry experiments were performed on a
859 QToF instrument (Synapt G2-Si, Waters Company, Manchester, UK). Calibration was performed using
860 sodium trifluoroacetate. The typical standard error was below 5 ppm. The native conditions used to
861 detect the intact tetramer require soft ionization parameters. Reliable and accurate detection of native
862 proteins were obtained by using an optimization procedure (Hall and Robinson 2012; Van der Rest and
863 Halgand 2017). In brief, for analysis under non-denaturing conditions the following instrumental
864 parameters were used: capillary voltage = 4.5 kV, sampling cone = 150 V, source offset, 150 V,
865 nebulization gas pressure = 5 bar, source temperature, 40 °C, desolvation temperature, 75 °C. Data
866 were processed with MassLynx.
867
868 **Reverse phase chromatography (RP) coupled to mass spectrometry (MS).**
869 Reverse phase chromatography was performed on an Acquity UPLC CSH C18 with a 2.0x100 mm.
870 Acetonitrile gradient was a linear increase of this last between 5 to 90 % in 35 min with a flow rate of 0.2

ml/min flow rate. Data were acquired on a Synapt instrument (Waters, Manchester, UK) equipped with an electrospray ionization source. In brief, instrumental parameters were the following: capillary voltage = 3.5 kV; source voltage = 50 V; source offset = 50 V; desolvation gas = 5 bar and desolvatation temperature was 650 °C. Calibration was performed using sodium trifluoroacetate. The typical standard error was below 5 ppm.

Author contributions

DM and CBA conceived the project. CBA and ABD conducted evolutionary analyses. DM, SAA and SC, CB performed samples preparation and biochemical characterization. DM and SMS analyzed thermal properties. CHL performed irradiation experiments. FH performed mass spectrometry measurements. DM and CBA wrote the first draft manuscript. All the authors analyzed the data and wrote the final manuscript.

Acknowledgment

Michel Lecocq, who initiated this work during his thesis but has since taken a non-academic path, deserves our warmest thanks. We would also like to thank Manolo Gouy for his advice, and Philippe Oger and priscilla Gillet for sharing unpublished information on the OGT of *Methanotorris formicicus*.

Funding

This work has been supported by the French National Research Agency. Projects i) ThermAdapt (ANR-22-CE02-0027) and ii) AlloSpace (ANR-21-CE44-0034-01). This project has also received financial support from the CNRS through the MITI interdisciplinary programs. This work used the platforms of the Grenoble Instruct-ERIC center (ISBG ; UAR 3518 CNRS-CEA-UGA-EMBL) within the Grenoble Partnership for Structural Biology (PSB), supported by FRISBI (ANR-10-INBS-0005-02) and GRAL, financed within the University Grenoble Alpes graduate school CBH-EUR-GS (ANR-17-EURE-0003). We thank Aline Le Roy and/or Christine Ebel, for assistance and/or access to the Analytical Ultracentrifugation (AUC) platform.

Conflict of interest

The authors declare that they have no conflicts of interest with the contents of this article. The data are available in the article and its online supplementary material.

Data Availability

The data underlying this article are available in the online supplementary material.

Bibliography

Akanuma S. 2017. Characterization of Reconstructed Ancestral Proteins Suggests a Change in Temperature of the Ancient Biosphere. Life (Basel) 7.

Amangeldina A, Tan ZW, Berezovsky IN. 2024. Living in trinity of extremes: Genomic and proteomic signatures of halophilic, thermophilic, and pH adaptation. Curr Res Struct Biol 7:100129.

Ando N, Barquera B, Bartlett DH, Boyd E, Burnim AA, Byer AS, Colman D, Gillilan RE, Gruebele M, Makhatadze G, et al. 2021. The Molecular Basis for Life in Extreme Environments. Annu Rev Biophys 50:343-372.

Bellack A, Huber H, Rachel R, Wanner G, Wirth R. 2011. Methanocaldococcus villosus sp. nov., a heavily flagellated archaeon that adheres to surfaces and forms cell-cell contacts. Int J Syst Evol Microbiol 61:1239-1245.

Bertrand Q, Coquille S, Iorio A, Sterpone F, Madern D. 2023. Biochemical, structural and dynamical characterizations of the lactate dehydrogenase from Selenomonas ruminantium provide information about an intermediate evolutionary step prior to complete allosteric regulation acquisition in the super family of lactate and malate dehydrogenases. J Struct Biol 215:108039.

Bigman LS, Levy Y. 2020. Proteins: molecules defined by their trade-offs. Curr Opin Struct Biol 60:50-56.

Birktoft JJ, Fernley RT, Bradshaw RA, Banaszak LJ. 1982. Amino acid sequence homology among the 2-hydroxy acid dehydrogenases: mitochondrial and cytoplasmic malate dehydrogenases form a homologous system with lactate dehydrogenase. Proc Natl Acad Sci U S A 79:6166-6170.

Blanquart S, Groussin M, Le Roy A, Szollosi GJ, Girard E, Franzetti B, Gouy M, Madern D. 2021. Resurrection of Ancestral Malate Dehydrogenases Reveals the Evolutionary History of Halobacterial Proteins: Deciphering Gene Trajectories and Changes in Biochemical Properties. Mol Biol Evol 38:3754-3774.

Boucher JI, Jacobowitz JR, Beckett BC, Classen S, Theobald DL. 2014. An atomic-resolution view of neofunctionalization in the evolution of apicomplexan lactate dehydrogenases. elife 3.

Boussau B, Blanquart S, Necsulea A, Lartillot N, Gouy M. 2008. Parallel adaptations to high temperatures in the Archaean eon. Nature 456:942-945.

Brochier-Armanet C, Madern D. 2021. Phylogenetics and biochemistry elucidate the evolutionary link between l-malate and l-lactate dehydrogenases and disclose an intermediate group of sequences with mix functional properties. Biochimie 191:140-153.

Burggraf S, Fricke H, Neuner A, Kristjansson J, Rouvier P, Mandelco L, Woese CR, Stetter KO. 1990. Methanococcus igneus sp. nov., a novel hyperthermophilic methanogen from a shallow submarine hydrothermal system. Syst Appl Microbiol 13:263-269.

Coker JA. 2019. Recent advances in understanding extremophiles. F1000Res 8.

Coquelle N, Fioravanti E, Weik M, Vellieux F, Madern D. 2007. Activity, stability and structural studies of lactate dehydrogenases adapted to extreme thermal environments. J Mol Biol 374:547-562.

Coquelle N, Talon R, Juers DH, Girard E, Kahn R, Madern D. 2010. Gradual adaptive changes of a protein facing high salt concentrations. J Mol Biol 404:493-505.

Dalhus B, Saarinen M, Sauer UH, Eklund P, Johansson K, Karlsson A, Ramaswamy S, Bjork A, Synstad B, Naterstad K, et al. 2002. Structural basis for thermophilic protein stability: structures of thermophilic and mesophilic malate dehydrogenases. J Mol Biol 318:707-721.

Daniel RM, Danson MJ. 2013. Temperature and the catalytic activity of enzymes: a fresh understanding. FEBS Lett 587:2738-2743.

Davlieva M, Shamoo Y. 2010. Crystal structure of a trimeric archaeal adenylate kinase from the mesophile Methanococcus maripaludis with an unusually broad functional range and thermal stability. Proteins 78:357-364.

Del Amparo R, Arenas M. 2022. Consequences of Substitution Model Selection on Protein Ancestral Sequence Reconstruction. Mol Biol Evol 39.
Donald JE, Kulp DW, DeGrado WF. 2011. Salt bridges: geometrically specific, designable interactions. Proteins 79:898-915.
Dong YW, Liao ML, Meng XL, Somero GN. 2018. Structural flexibility and protein adaptation to temperature: Molecular dynamics analysis of malate dehydrogenases of marine molluscs. Proc Natl Acad Sci U S A 115:1274-1279.
Dray S, Dufour A-B. 2007. Theade4Package: Implementing the Duality Diagram for Ecologists. Journal of Statistical Software 22:1-20.
Dutheil J, Boussau B. 2008. Non-homogeneous models of sequence evolution in the Bio++ suite of libraries and programs. BMC Evol Biol 8:255.
Dutta C, Paul S. 2012. Microbial lifestyle and genome signatures. Curr Genomics 13:153-162.
Echave J, Spielman SJ, Wilke CO. 2016. Causes of evolutionary rate variation among protein sites. Nat Rev Genet 17:109-121.
Eme L, Tamarit D, Caceres EF, Stairs CW, De Anda V, Schon ME, Seitz KW, Dombrowski N, Lewis WH, Homa F, et al. 2023. Inference and reconstruction of the heimdallarchaeial ancestry of eukaryotes. Nature 618:992-999.
Feller G. 2010. Protein stability and enzyme activity at extreme biological temperatures. J Phys Condens Matter 22:323101.
Felsenstein J. 1985. Phylogenies and the Comparative Method. The american naturalist 125:1-15.
Feng Y, Ping Tan C, Zhou C, Yagoub AEA, Xu B, Sun Y, Ma H, Xu X, Yu X. 2020. Effect of freeze-thaw cycles pretreatment on the vacuum freeze-drying process and physicochemical properties of the dried garlic slices. Food Chem 324:126883.
Furukawa R, Toma W, Yamazaki K, Akanuma S. 2020. Ancestral sequence reconstruction produces thermally stable enzymes with mesophilic enzyme-like catalytic properties. Sci Rep 10:15493.
Fusco G, Bemporad F, Chiti F, Dobson CM, De Simone A. 2022. The role of structural dynamics in the thermal adaptation of hyperthermophilic enzymes. Front Mol Biosci 9:981312.
Garcia AK, Kacar B. 2019. How to resurrect ancestral proteins as proxies for ancient biogeochemistry. Free Radic Biol Med 140:260-269.
Garcia AK, Schopf JW, Yokobori SI, Akanuma S, Yamagishi A. 2017. Reconstructed ancestral enzymes suggest long-term cooling of Earth's photic zone since the Archean. Proc Natl Acad Sci U S A 114:4619-4624.
Gaucher EA, Govindarajan S, Ganesh OK. 2008. Palaeotemperature trend for Precambrian life inferred from resurrected proteins. Nature 451:704-707.
Gaucher EA, Thomson JM, Burgan MF, Benner SA. 2003. Inferring the paleoenvironment of ancient bacteria on the basis of resurrected proteins. Nature 425:285-288.
Goihberg E, Dym O, Tel-Or S, Levin I, Peretz M, Burstein Y. 2007. A single proline substitution is critical for the thermostabilization of Clostridium beijerinckii alcohol dehydrogenase. Proteins 66:196-204.
Goldstein RA. 2011. The evolution and evolutionary consequences of marginal thermostability in proteins. Proteins 79:1396-1407.
Grafen A. 1989. The phylogenetic regression. Philos Trans R Soc Lond B Biol Sci 326:119-157.
Gribaldo S, Philippe H. 2002. Ancient phylogenetic relationships. Theor Popul Biol 61:391-408.
Groussin M, Boussau B, Gouy M. 2013. A branch-heterogeneous model of protein evolution for efficient inference of ancestral sequences. Syst Biol 62:523-538.
Groussin M, Gouy M. 2011. Adaptation to environmental temperature is a major determinant of molecular evolutionary rates in archaea. Mol Biol Evol 28:2661-2674.
Halgand F, Houee-Levin C, Weik M, Madern D. 2020. Remote oxidative modifications induced by oxygen free radicals modify T/R allosteric equilibrium of a hyperthermophilic lactate dehydrogenase. J Struct Biol 210:107478.
Hall Z, Robinson CV. 2012. Do charge state signatures guarantee protein conformations? J Am Soc Mass Spectrom 23:1161-1168.
Hicks M, Gebicki JM. 2001. Rate constants for reaction of hydroxyl radicals with Tris, Tricine and Hepes buffers. FEBS Lett 199:92-94.
Houee-Levin C, Bobrowski K. 2013. The use of the methods of radiolysis to explore the mechanisms of free radical modifications in proteins. J Proteomics 92:51-62.
Huber H, Thomm M, Konig H, Thies G, Stetter KO. 1982. Methanococcus thermolithotrophicus, a novel thermophilic lithotrophic methanogen. Arch Microbiol 132:47-50.
Iglhaut C, Pecerska J, Gil M, Anisimova M. 2024. Please Mind the Gap: Indel-Aware Parsimony for Fast and Accurate Ancestral Sequence Reconstruction and Multiple Sequence Alignment Including Long Indels. Mol Biol Evol 41.

Iorio A, Roche J, Engilberge S, Coquelle N, Girard E, Sterpone F, Madern D. 2021. Biochemical, structural and dynamical studies reveal strong differences in the thermal-dependent allosteric behavior of two extremophilic lactate dehydrogenases. J Struct Biol 213:107769.
Irimia A, Madern D, Zaccai G, Vellieux FM. 2004. Methanoarchaeal sulfolactate dehydrogenase: prototype of a new family of NADH-dependent enzymes. EMBO J 23:1234-1244.
Irimia A, Vellieux FM, Madern D, Zaccai G, Karshikoff A, Tibbelin G, Ladenstein R, Lien T, Birkeland NK. 2004. The 2.9A resolution crystal structure of malate dehydrogenase from Archaeoglobus fulgidus: mechanisms of oligomerisation and thermal stabilisation. J Mol Biol 335:343-356.
Jeanthon C, L'Haridon S, Reysenbach AL, Vernet M, Messner P, Sleytr UB, Prieur D. 1998. Methanococcus infernus sp. nov., a novel hyperthermophilic lithotrophic methanogen isolated from a deep-sea hydrothermal vent. Int J Syst Bacteriol 48 Pt 3:913-919.
Jones WJ, Leigh JA, Mayer F, Woese CR, Wolfe RS. 1983. Methanococcus-Jannaschii Sp-Nov, an Extremely Thermophilic Methanogen from a Submarine Hydrothermal Vent. Arch Microbiol 136:254-261.
Jowkar G, Pecerska J, Maiolo M, Gil M, Anisimova M. 2023. ARPIP: Ancestral Sequence Reconstruction with Insertions and Deletions under the Poisson Indel Process. Syst Biol 72:307-318.
Kalimeri M, Girard E, Madern D, Sterpone F. 2014. Interface matters: the stiffness route to stability of a thermophilic tetrameric malate dehydrogenase. PLoS One 9:e113895.
Kalyaanamoorthy S, Minh BQ, Wong TKF, von Haeseler A, Jermiin LS. 2017. ModelFinder: fast model selection for accurate phylogenetic estimates. Nat Methods 14:587-589.
Katava M, Marchi M, Madern D, Sztucki M, Maccarini M, Sterpone F. 2020. Temperature Unmasks Allosteric Propensity in a Thermophilic Malate Dehydrogenase via Dewetting and Collapse. J Phys Chem B 124:1001-1008.
Katoh K, Standley DM. 2013. MAFFT multiple sequence alignment software version 7: improvements in performance and usability. Mol Biol Evol 30:772-780.
Kawakami R, Sakuraba H, Goda S, Tsuge H, Ohshima T. 2009. Refolding, characterization and crystal structure of (S)-malate dehydrogenase from the hyperthermophilic archaeon Aeropyrum pernix. Biochim Biophys Acta 1794:1496-1504.
Kendall MM, Liu Y, Sieprawska-Lupa M, Stetter KO, Whitman WB, Boone DR. 2006. Methanococcus aeolicus sp. nov., a mesophilic, methanogenic archaeon from shallow and deep marine sediments. Int J Syst Evol Microbiol 56:1525-1529.
Knop JM, Mukherjee S, Jaworek MW, Kriegler S, Manisegaran M, Fetahaj Z, Ostermeier L, Oliva R, Gault S, Cockell CS, et al. 2023. Life in Multi-Extreme Environments: Brines, Osmotic and Hydrostatic Pressure horizontal line A Physicochemical View. Chem Rev 123:73-104.
Koenekoop L, Aqvist J. 2023. Principles of Cold Adaptation of Fish Lactate Dehydrogenases Revealed by Computer Simulations of the Catalytic Reaction. Mol Biol Evol 40.
Kurokawa M, Higashi K, Yoshida K, Sato T, Maruyama S, Mori H, Kurokawa K. 2023. Metagenomic Thermometer. DNA Res 30.
Kurr M, Huber R, König H, Jannasch HW, Fricke H, Trincone A, Kristjansson JK, Stetter KO. 1991. Methanopyrus kandleri, gen. and sp. nov. represents a novel group of hyperthermophilic methanogens, growing at 110°C. Arch. Microbiol. 156:239-247.
Lamolle G, Simon D, Iriarte A, Musto H. 2023. Main Factors Shaping Amino Acid Usage Across Evolution. J Mol Evol 91:382-390.
Lecocq M, Groussin M, Gouy M, Brochier-Armanet C. 2021. The Molecular Determinants of Thermoadaptation: Methanococcales as a Case Study. Mol Biol Evol 38:1761-1776.
Lu Z, Xia R, Zhang S, Pan J, Liu Y, Wolf YI, Koonin EV, Li M. 2024. Evolution of optimal growth temperature in Asgard archaea inferred from the temperature dependence of GDP binding to EF-1A. Nat Commun 15:515.
Madern D. 2002. Molecular evolution within the L-malate and L-lactate dehydrogenase super-family. J Mol Evol 54:825-840.
Maffucci I, Laage D, Sterpone F, Stirnemann G. 2020. Thermal Adaptation of Enzymes: Impacts of Conformational Shifts on Catalytic Activation Energy and Optimum Temperature. Chemistry 26:10045-10056.
Martins EP, Hansen TF. 1997. Phylogenies and the comparative method: A general approach to incorporating phylogenetic information onto the analysis of interspecific data. American Naturalist 149:646-667.
McCue WM, Finzel BC. 2022. Structural Characterization of the Human Cytosolic Malate Dehydrogenase I. ACS Omega 7:207-214.
Mehta MP, Baross JA. 2006. Nitrogen fixation at 92 degrees C by a hydrothermal vent archaeon. Science 314:1783-1786.

Merino N, Aronson HS, Bojanova DP, Feyhl-Buska J, Wong ML, Zhang S, Giovannelli D. 2019. Living at the Extremes: Extremophiles and the Limits of Life in a Planetary Context. Front Microbiol 10:780.
Michetti D, Brandsdal BO, Bon D, Isaksen GV, Tiberti M, Papaleo E. 2017. A comparative study of cold- and warm-adapted Endonucleases A using sequence analyses and molecular dynamics simulations. PLoS One 12:e0169586.
Naser-Khdour S, Minh BQ, Zhang W, Stone EA, Lanfear R. 2019. The Prevalence and Impact of Model Violations in Phylogenetic Analysis. Genome Biol Evol 11:3341-3352.
Nguyen LT, Schmidt HA, von Haeseler A, Minh BQ. 2015. IQ-TREE: a fast and effective stochastic algorithm for estimating maximum-likelihood phylogenies. Mol Biol Evol 32:268-274.
Nguyen V, Wilson C, Hoemberger M, Stiller JB, Agafonov RV, Kutter S, English J, Theobald DL, Kern D. 2017. Evolutionary drivers of thermoadaptation in enzyme catalysis. Science 355:289-294.
Paradis E, Schliep K. 2019. ape 5.0: an environment for modern phylogenetics and evolutionary analyses in R. Bioinformatics 35:526-528.
Perez-Jimenez R, Ingles-Prieto A, Zhao ZM, Sanchez-Romero I, Alegre-Cebollada J, Kosuri P, Garcia-Manyes S, Kappock TJ, Tanokura M, Holmgren A, et al. 2011. Single-molecule paleoenzymology probes the chemistry of resurrected enzymes. Nat Struct Mol Biol 18:592-596.
Pikuta EV, Hoover RB, Tang J. 2007. Microbial extremophiles at the limits of life. Crit Rev Microbiol 33:183-209.
Pinheiro J, Bates D. 2024. nlme: Linear and Nonlinear Mixed Effects Models.
Pinney MM, Mokhtari DA, Akiva E, Yabukarski F, Sanchez DM, Liang R, Doukov T, Martinez TJ, Babbitt PC, Herschlag D. 2021. Parallel molecular mechanisms for enzyme temperature adaptation. Science 371.
Prajapati RS, Das M, Sreeramulu S, Sirajuddin M, Srinivasan S, Krishnamurthy V, Ranjani R, Ramakrishnan C, Varadarajan R. 2007. Thermodynamic effects of proline introduction on protein stability. Proteins 66:480-491.
Prondzinsky P, Toyoda S, McGlynn SE. 2023. The methanogen core and pangenome: conservation and variability across biology's growth temperature extremes. DNA Res 30.
Richard SB, Madern D, Garcin E, Zaccai G. 2000. Halophilic adaptation: novel solvent protein interactions observed in the 2.9 and 2.6 A resolution structures of the wild type and a mutant of malate dehydrogenase from Haloarcula marismortui. Biochemistry 39:992-1000.
Risso VA, Gavira JA, Mejia-Carmona DF, Gaucher EA, Sanchez-Ruiz JM. 2013. Hyperstability and substrate promiscuity in laboratory resurrections of Precambrian beta-lactamases. J Am Chem Soc 135:2899-2902.
Robin AY, Brochier-Armanet C, Bertrand Q, Barette C, Girard E, Madern D. 2023. Deciphering Evolutionary Trajectories of Lactate Dehydrogenases Provides New Insights into Allostery. Mol Biol Evol 40.
Roche J, Girard E, Mas C, Madern D. 2019. The archaeal LDH-like malate dehydrogenase from Ignicoccus islandicus displays dual substrate recognition, hidden allostery and a non-canonical tetrameric oligomeric organization. J Struct Biol 208:7-17.
Rothschild LJ, Mancinelli RL. 2001. Life in extreme environments. Nature 409:1092-1101.
Sakai S, Takaki Y, Miyazaki M, Ogawara M, Yanagawa K, Miyazaki J, Takai K. 2019. Methanofervidicoccus abyssi gen. nov., sp. nov., a hydrogenotrophic methanogen, isolated from a hydrothermal vent chimney in the Mid-Cayman Spreading Center, the Caribbean Sea. Int J Syst Evol Microbiol 69:1225-1230.
Sammond DW, Kastelowitz N, Himmel ME, Yin H, Crowley MF, Bomble YJ. 2016. Comparing Residue Clusters from Thermophilic and Mesophilic Enzymes Reveals Adaptive Mechanisms. PLoS One 11:e0145848.
Sauer DB, Wang DN. 2019. Predicting the optimal growth temperatures of prokaryotes using only genome derived features. Bioinformatics 35:3224-3231.
Schwartz SL, Garcia AK, Kacar B, Fournier GP. 2022. Early Nitrogenase Ancestors Encompassed Novel Active Site Diversity. Mol Biol Evol 39.
Selberg AGA, Gaucher EA, Liberles DA. 2021. Ancestral Sequence Reconstruction: From Chemical Paleogenetics to Maximum Likelihood Algorithms and Beyond. J Mol Evol 89:157-164.
Shimozawa Y, Matsuhisa H, Nakamura T, Himiyama T, Nishiya Y. 2022. Reducing substrate inhibition of malate dehydrogenase from Geobacillus stearothermophilus by C-terminal truncation. Protein Eng Des Sel 35.
Smole Z, Nikolic N, Supek F, Smuc T, Sbalzarini IF, Krisko A. 2011. Proteome sequence features carry signatures of the environmental niche of prokaryotes. BMC Evol Biol 11:26.
Spinks JWT, Woods RJ. 1990. An introduction to radiation chemistry. New York, Toronto: John-Wiley and Sons.

Takai K, Inoue A, Horikoshi K. 2002. Methanothermococcus okinawensis sp. nov., a thermophilic, methane-producing archaeon isolated from a Western Pacific deep-sea hydrothermal vent system. Int J Syst Evol Microbiol 52:1089-1095.
Takai K, Nealson KH, Horikoshi K. 2004. Methanotorris formicicus sp. nov., a novel extremely thermophilic, methane-producing archaeon isolated from a black smoker chimney in the Central Indian Ridge. Int J Syst Evol Microbiol 54:1095-1100.
Talon R, Coquelle N, Madern D, Girard E. 2014. An experimental point of view on hydration/solvation in halophilic proteins. Front Microbiol 5:66.
Tehei M, Madern D, Franzetti B, Zaccai G. 2005. Neutron scattering reveals the dynamic basis of protein adaptation to extreme temperature. J Biol Chem 280:40974-40979.
Tian J, Wang P, Gao S, Chu X, Wu N, Fan Y. 2010. Enhanced thermostability of methyl parathion hydrolase from Ochrobactrum sp. M231 by rational engineering of a glycine to proline mutation. Febs J 277:4901-4908.
Touchon M, Perrin A, de Sousa JAM, Vangchhia B, Burn S, O'Brien CL, Denamur E, Gordon D, Rocha EP. 2020. Phylogenetic background and habitat drive the genetic diversification of Escherichia coli. PLoS Genet 16:e1008866.
Trudeau DL, Kaltenbach M, Tawfik DS. 2016. On the Potential Origins of the High Stability of Reconstructed Ancestral Proteins. Mol Biol Evol 33:2633-2641.
Tule S, Foley G, Zhao C, Forbes M, Boden M. 2024. Optimal phylogenetic reconstruction of insertion and deletion events. Bioinformatics 40:i277-i286.
Valiev M, D'Auria R, Tobias DJ, Garrett BC. 2009. Interactions of Cl- and OH radical in aqueous solution. J Phys Chem A 113:8823-8825.
Vallina Estrada E, Oliveberg M. 2022. Physicochemical classification of organisms. Proc Natl Acad Sci U S A 119:e2122957119.
Van der Rest G, Halgand F. 2017. Size Exclusion Chromatography-Ion Mobility-Mass Spectrometry Coupling: a Step Toward Structural Biology. J Am Soc Mass Spectrom 28:2519-2522.
Wheeler LC, Lim SA, Marqusee S, Harms MJ. 2016. The thermostability and specificity of ancient proteins. Curr Opin Struct Biol 38:37-43.
Whitman WB, Boone DR, Koga K. 2015. Methanococcales. In. Bergey's Manual of Systematics of Archaea and Bacteria. Chichester, UK: John Wiley & Sons.
Williams PD, Pollock DD, Blackburne BP, Goldstein RA. 2006. Assessing the accuracy of ancestral protein reconstruction methods. PLoS Comput Biol 2:e69.
Wrabl JO, Gu J, Liu T, Schrank TP, Whitten ST, Hilser VJ. 2011. The role of protein conformational fluctuations in allostery, function, and evolution. Biophys Chem 159:129-141.
Xie GF, Tsou CL. 1987. Conformational and activity changes during guanidine denaturation of D-glyceraldehyde-3-phosphate dehydrogenase. Biochim Biophys Acta 911:19-24.
Yao QZ, Tian M, Tsou CL. 1984. Comparison of the rates of inactivation and conformational changes of creatine kinase during urea denaturation. Biochemistry 23:2740-2744.
Yu H, Dalby PA. 2018. Exploiting correlated molecular-dynamics networks to counteract enzyme activity-stability trade-off. Proc Natl Acad Sci U S A 115:E12192-E12200.
Zaucha J, Heddle JG. 2017. Resurrecting the Dead (Molecules). Comput Struct Biotechnol J 15:351-358.
Zeikus JG, Wolfe RS. 1972. Methanobacterium thermoautotrophicus sp. n., an anaerobic, autotrophic, extreme thermophile. J Bacteriol 109:707-715.
Zeldovich KB, Berezovsky IN, Shakhnovich EI. 2007. Protein and DNA sequence determinants of thermophilic adaptation. PLoS Comput Biol 3:e5.
Zhang YL, Zhou JM, Tsou CL. 1993. Inactivation precedes conformation change during thermal denaturation of adenylate kinase. Biochim Biophys Acta 1164:61-67.
Zhou C, Xue Y, Ma Y. 2010. Enhancing the thermostability of alpha-glucosidase from Thermoanaerobacter tengcongensis MB4 by single proline substitution. J Biosci Bioeng 110:12-17.